AD-A193 844 OPTIMIZED OBSERVATION PERIODS REQUIRED TO ACHIEVE GEODETIC ACCURACIES USING THE GLOBAL POSITIONING SYSTEM (U) NAVAL POSTGRADUATE SCHOOL MONTEREY CA R H BOUCHARD 1/1

UNCLASSIFIED MAR 88 F/G 17/7 NL

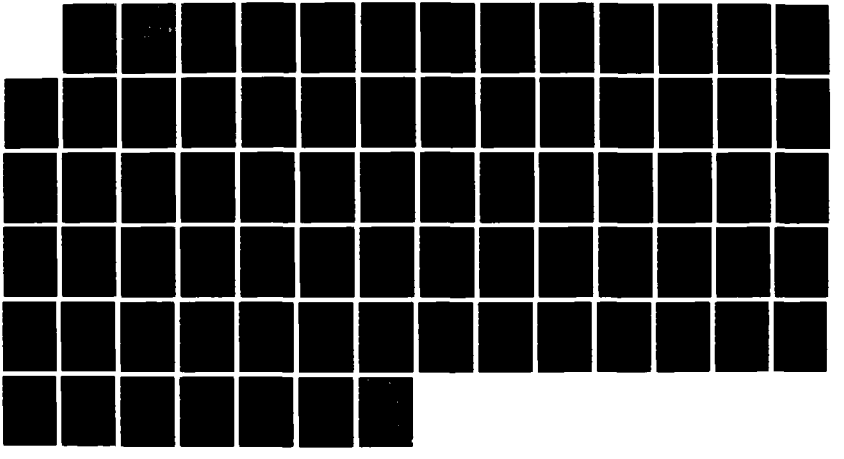

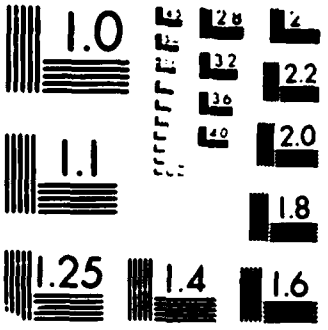

MICROCOPY RESOLUTION TEST CHART

NAVAL POSTGRADUATE SCHOOL

Monterey, California

THESIS

OPTIMIZED OBSERVATION PERIODS
REQUIRED TO ACHIEVE GEODETIC ACCURACIES
USING THE GLOBAL POSITIONING SYSTEM

by

Richard H. Bouchard

March 1988

Co-Advisor — Stevens P. Tucker
Co-Advisor — Narendra K. Saxena

Unclassified

security classification of this page

REPORT DOCUMENTATION PAGE

1a Report Security Classification: Unclassified	1b Restrictive Markings
2a Security Classification Authority	3 Distribution/Availability of Report: Approved for public release; distribution is unlimited.
2b Declassification/Downgrading Schedule	
4 Performing Organization Report Number(s)	5 Monitoring Organization Report Number(s)
6a Name of Performing Organization: Naval Postgraduate School	6b Office Symbol (if applicable): 35
7a Name of Monitoring Organization: Naval Postgraduate School	
6c Address (city, state, and ZIP code): Monterey, CA 93943-5000	7b Address (city, state, and ZIP code): Monterey, CA 93943-5000
8a Name of Funding/Sponsoring Organization	8b Office Symbol (if applicable)
9 Procurement Instrument Identification Number	
8c Address (city, state, and ZIP code)	10 Source of Funding Numbers: Program Element No. / Project No. / Task No. / Work Unit Accession No.

11 Title (include security classification): OPTIMIZED OBSERVATION PERIODS REQUIRED TO ACHIEVE GEODETIC ACCURACIES USING THE GLOBAL POSITIONING SYSTEM

12 Personal Author(s): Richard H. Bouchard

13a Type of Report	13b Time Covered	14 Date of Report (year, month, day)	15 Page Count
Master's Thesis	From To	March 1988	74

16 Supplementary Notation: The views expressed in this thesis are those of the author and do not reflect the official policy or position of the Department of Defense or the U.S. Government.

17 Cosati Codes			18 Subject Terms (continue on reverse if necessary and identify by block number)
Field	Group	Subgroup	Global Positioning System, relative geodesy, Trimble 4000SX, long baseline determination, triple difference, GPS, PDOP, optimized observing periods, geodetic accuracy.

19 Abstract (continue on reverse if necessary and identify by block number)

Measurements of a 1230-km baseline were made during an eight-week period in the fall of 1987 using Trimble 4000SX single-frequency, five channel Global Positioning System (GPS) receivers. Twenty-eight days of carrier phase data were processed using correlated triple differences with fixed satellite orbits, the broadcast ephemerides, a modified Hopfield tropospheric model, and without ionospheric correction to determine the accuracies and precisions of the slope distance and baseline components. The data were processed in ever increasing observing sessions to determine the optimized observation periods required to achieve various orders of geodetic accuracies.

The accuracies of the slope distances were better than 1.0 ppm for any observing period. The day-to-day repeatabilities of the slope distance measurements were better than 1.0 ppm (2σ) after 20 minutes of observations. Accuracies and repeatabilities (2σ) of the baseline components were better than 10.0 ppm after 20 minutes of observations. The correlated triple difference results were on the order of previous GPS surveys that used higher resolution differencing or external timing aids. Discussions include the effects of ephemeris, tropospheric and ionospheric errors, and dilution of precision.

Observation periods and mean slope distance errors were reduced when observations started close to and included the infinite peak of the Position Dilution of Precision (PDOP). The smallest variances were associated with observations about the infinite PDOP peak.

20 Distribution/Availability of Abstract	21 Abstract Security Classification	
☒ unclassified/unlimited ☐ same as report ☐ DTIC users	Unclassified	
22a Name of Responsible Individual: Stevens P. Tucker	22b Telephone (include Area code): (408)-646-3269	22c Office Symbol: 68Tx

DD FORM 1473,84 MAR 83 APR edition may be used until exhausted. All other editions are obsolete.

security classification of this page

Unclassified

Approved for public release; distribution is unlimited.

Optimized Observation Periods
Required to Achieve Geodetic Accuracies
Using the Global Positioning System

by

Richard H. Bouchard
Lieutenant, United States Navy
B.S., Lyndon State College, 1979

Submitted in partial fulfillment of the
requirements for the degree of

MASTER OF SCIENCE IN METEOROLOGY AND OCEANOGRAPHY

from the

NAVAL POSTGRADUATE SCHOOL
March 1988

Author: Richard H. Bouchard

Richard H. Bouchard

Approved by: Stevens P. Tucker

Stevens P. Tucker, Co-Advisor

Narendra K. Saxena, Co-Advisor

Curtis A. Collins, Chairman,
Department of Oceanography

Gordon E. Schacher,
Dean of Science and Engineering

ABSTRACT

Measurements of a 1230-km baseline were made during an eight-week period in the fall of 1987 using Trimble 4000SX single-frequency, five channel Global Positioning System (GPS) receivers. Twenty-eight days of carrier phase data were processed using correlated triple differences with fixed satellite orbits, the broadcast ephemerides, a modified Hopfield tropospheric model, and without ionospheric correction to determine the accuracies and precisions of the slope distance and baseline components. The data were processed in ever increasing observing sessions to determine the optimized observation periods required to achieve various orders of geodetic accuracies.

The accuracies of the slope distances were better than 1.0 ppm for any observing period. The day-to-day repeatabilities of the slope distance measurements were better than 1.0 ppm (2σ) after 20 minutes of observations. Accuracies and repeatabilities (2σ) of the baseline components were better than 10.0 ppm after 20 minutes of observations. The correlated triple difference results were on the order of previous GPS surveys that used higher resolution differencing or external timing aids. Discussions include the effects of ephemeris, tropospheric and ionospheric errors, and dilution of precision.

Observation periods and mean slope distance errors were reduced when observations started close to and included the infinite peak of the Position Dilution of Precision (PDOP). The smallest variances were associated with observations about the infinite PDOP peak.

TABLE OF CONTENTS

LIST OF TABLES

LIST OF FIGURES

LIST OF SYMBOLS

b	Baseline distance (slope distance)
b_M	Measured baseline distance
b_T	True baseline distance
c	Speed of light
d	Day
e	Elevation angle
f	Frequency
h	Highest satellite
i	Observation epoch identifier
l	Integer number of epochs
n	Refractivity
n_i	Number of epochs
n_s	Number of satellites
r	Receiver identifier
s	Satellite identifier
v	Angle between the vector tangent to the ellipsoid and the slope distance vector
A(r,s,i)	Initial integer ambiguity
C	Component or coordinate
DD(h,s,i)	Double difference
E	Error
$\overline{E}$	Mean error
M_{TD}	Maximum number of triple difference observations
N	Refractive index
SD(s,i)	Single difference
TD(i)	Triple difference
X	X coordinate
Y	Y coordinate
Z	Z coordinate
$\delta(i)$	Difference between receiver clock times

γ	Angle between slant range vectors from a satellite to two ground stations
ϕ	Phase of the GPS carrier signal
ρ	Satellite-receiver slant range
$\dot{\rho}$	Time rate of change of ρ
σ	Standard deviation
$\tau(r,t)$	Tropospheric delay
θ	Angle between the slope distance vector and the elevation angle to a satellite
$\xi(t)$	Average offset of receiver clock time
$\zeta(r,t)$	Common receiver clock errors
Δ	Difference
ΔX	Baseline component in the X direction
ΔY	Baseline component in the Y direction
ΔZ	Baseline component in the Z direction

LIST OF ABBREVIATIONS AND ACRONYMS

ppm	parts per million
AODE	Age of Data (Ephemeris)
C/A	Coarse Acquisition Code
DMA	Defense Mapping Agency
DMAHTC	DMA Hydrographic Topographic Center
DOD	Department of Defense
EF	Electron Fluence
GDOP	Geometric Dilution of Precision
GPS	Global Positioning System
MRY	Monterey GPS antenna location
NAD83	North American Datum 1983
NGS	National Geodetic Survey
NOAA	National Oceanic and Atmospheric Administration
NPS	Naval Postgraduate School
Ob	Observing or observation
PDOP	Position Dilution of Precision
PST	Pacific Standard Time (+8 hours UTC)
SEA-TAC	Seattle-Tacoma International Airport
SPt	Sand Point GPS antenna location
SV	Satellite Vehicle
TDOP	Time Dilution of Precision
TEC	Total Electron Content
TOW	Time Of the Week
UTC	Universal Coordinated Time
VLBI	Very Long Baseline Interferometry
WGS84	World Geodetic System 1984
WSO	National Weather Service Office

I. INTRODUCTION

A priori knowledge of the observation periods required to achieve specified orders of geodetic accuracies is important in planning efficient and productive geodetic surveys. While terrestrial surveys have specified field and processing procedures and standards to categorize the geodetic accuracies of surveys [Federal Geodetic Control Committee, 1984], only recently have standards been *proposed* for surveys conducted with the Global Positioning System (GPS) [Federal Geodetic Control Committee, 1986]. Among the proposed requirements are standards for the length of observing periods and satellite geometry.

Field studies by Remondi [1984] and numerical simulations by Fell [1980], Langley *et al.* [1984], and Landau and Eissfeller [1986] studied optimized observation periods, but for baselines less than 100 km. Cannon *et al.* [1985], Bock *et al.* [1984], Goad *et al.* [1985], Mader and Abell [1985], and Bertiger and Lichten [1987] conducted long baseline surveys, but did not study optimized observation periods. One of the objectives of this thesis is to fill the gap between the above studies, *i.e.*, examine the optimized observation periods for a long baseline.

The optimized times will be examined using the correlated triple difference carrier beat phase observable because of its insensitivity to integer ambiguities and loss of lock of the GPS carrier by the receiver. Another objective of this thesis is to add to the body of triple difference accuracy testing following a recommendation by Remondi [1984, p. 259]: "More testing is required to establish the full accuracy potential of the triple difference method."

GPS carrier phase and pseudorange measurements were made during an eight-week period in the fall of 1987 with Trimble 4000SX single-frequency, 5 channel receivers. The long baseline is approximately 1230 km in length between the National Oceanic and Atmospheric Administration's (NOAA) Western Regional Center located at Sand Point in Seattle, Washington, and the Naval Postgraduate School (NPS), Monterey, California. The baseline was determined by locating the positions of its ends by connecting them by independent short baseline surveys from nearby Very Long Baseline Interferometry (VLBI) horizontal control points. The results of those surveys form the reference to which accuracy will be determined.

Additionally, studies for repeatability were conducted following another recommendation by Remondi [1984, p. 263] to enhance the capabilities of GPS measurements. The recommendation was to perform extensive repeatability studies on non-varying baselines for verifying and improving the GPS modelling.

II. BASELINE DETERMINATION USING GPS

A. INTRODUCTION

The Department of Defense's (DOD) Global Positioning System is intended to provide accurate positioning and precise timing for navigation purposes by broadcasting codes superimposed on two radio carrier frequencies from satellites. The satellites are placed in a constellation so that at least four satellites are visible globally. The Precise Code (P code) will be limited to authorized DOD users. The Coarse Acquisition (C A) code provides real-time accuracies to about 100 m [Baker, 1986] and is available to anyone.

The codes provide their transmit times, satellite orbit and clock information, and information to enable any receiver to lock onto other GPS satellites. The orbital information (ephemeris) provides the position of the satellite. The receiver measures the time delay between the receipt of the C A code and its transmission time. The time delay can be transformed into an apparent slant range from the satellite's known position to determine the location of the receiver. Since it includes delays due to receiver clock errors and the effects of atmospheric refraction, the apparent slant range is referred to as the *pseudorange*. A minimum of four satellites are required to solve the system of range equations for the receiver's coordinates and clock errors.

While the C A code provides real-time location, it does not meet the accuracy required for precise geodetic work. Nevertheless, GPS makes possible a higher resolution via the carrier signal. Though the carrier itself does not contain the orbital and timing information, which would have to be supplied by some other means, it does offer a higher resolution because of its 19-cm wavelength

B. THE MONTEREY-SAND POINT BASELINE

1. General

The length of the Monterey-Sand Point baseline (Figure 1) was computed by differencing the World Geodetic System 1984 (WGS84) [Defense Mapping Agency, 1987] Cartesian coordinates determined for Monterey and Sand Point by short baseline GPS surveys from known horizontal control points. The precision and agreement with terrestrial survey results of short baseline GPS measurements using single frequency, double difference solutions are well documented (*e.g.*, [Remondi, 1984], [Goad and Remondi, 1984], [Bock *et al.*, 1984]).

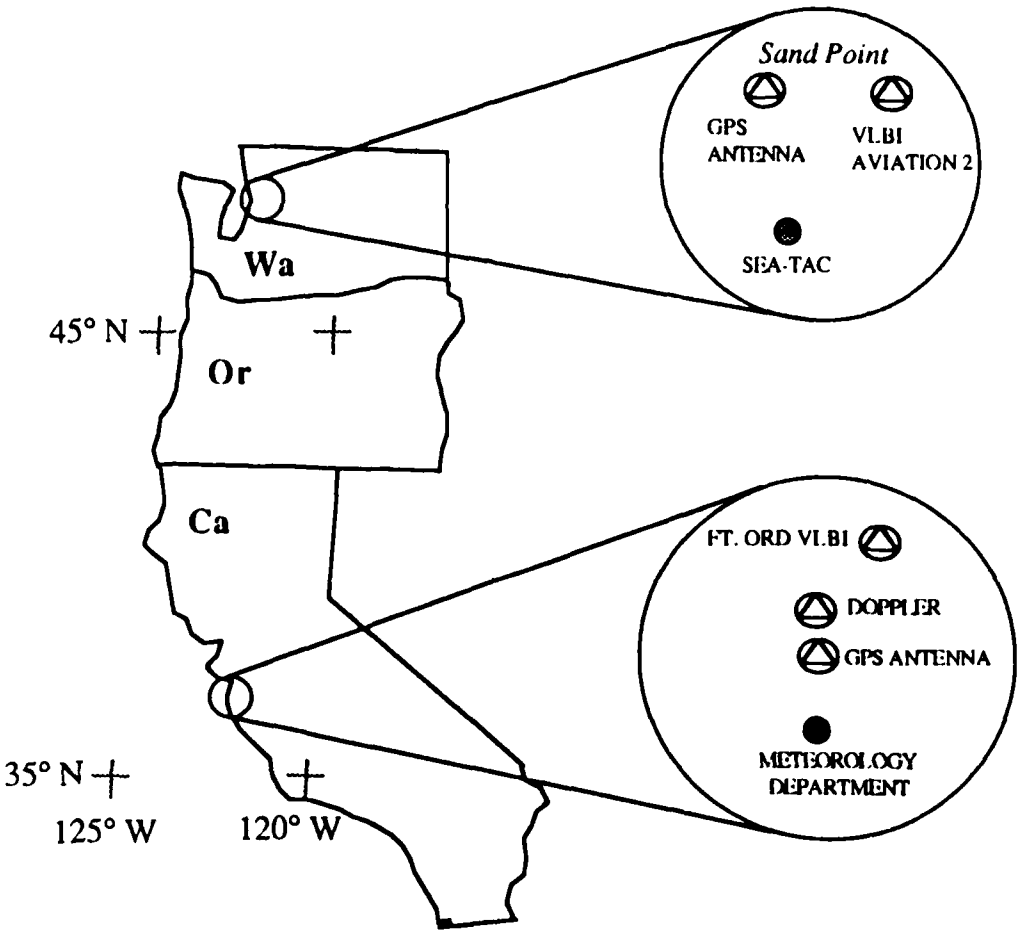

Figure 1. Monterey-Sand Point Baseline and environs: Insets not drawn to scale.

At Sand Point, on-site meteorological measurements were made near the middle of the observing session. For the Monterey antenna determination meteorological measurements were made every half hour and the mean of all the measurements was used in the processing. The *Trim640* solutions were obtained using uncorrelated double differences and estimating initial integer ambiguities. The ambiguities were fixed to the

integer values that produced the smallest residuals. A tropospheric factor was estimated along with the integer ambiguities and the baseline components in the least-squares processing.

The horizontal control points used for the reference stations in determining the coordinates of the antennas were mobile Very Long Baseline Interferometry (VLBI) sites. The NAD83 Cartesian coordinates for the VLBI sites were provided by the the Gravity, Astronomy and Space Geodesy Branch of the National Geodetic Survey (NGS) [Abell, 1987]. The NAD83 coordinates were determined in August 1987 from a global adjustment of VLBI surveys. Carter *et al.* [1985] described the NGS VLBI program. The Defense Mapping Agency Hydrographic Topographic Office (DMAHTC) validated the direct transformation of the VLBI Cartesian coordinates to WGS84 Cartesian coordinates [Kumar, 1988].

2. Monterey Coordinates

The coordinates for the Monterey antenna location were determined by averaging two surveys conducted on separate days from the VLBI site FT ORD NCMN 1981. Table 1 lists the observing sessions used to determine the WGS84 coordinates of the Monterey antenna. Table 2 lists the results of the GPS surveys.

Table 1. MONTEREY ANTENNA LOCATION SURVEYS: From FT ORD NCMN 1981. PST = Pacific Standard Time.

Date	Start Time (PST)	End Time (PST)	Number of Double Difference Observations	Percent Rejected	Slope Distance (m)	σ_b
09 16 87	1018	1210	996	7	12139.8125	0.025
09 18 87	0914	1120	1136	4	12139.8119	0.025

The Monterey coordinates were computed from:

$$C_{MRY} = C_{ORD} + \overline{\Delta}_c$$

where:

C_{MRY}	Monterey coordinate
C_{ORD}	Ft Ord coordinate
$\overline{\Delta}_c$	Variance-weighted mean baseline component

The uncertainties of the Monterey coordinates, $\sigma_{C_{MRY}}$, were computed from:

Table 2. RESULTS OF MONTEREY ANTENNA LOCATION SURVEYS: WGS84 Cartesian Coordinates (meters).

DATE	FT ORD X	$\sigma_{ORD\,X}$	ΔX	$\sigma_{\Delta X}$	MRY X	$\sigma_{MRY\,X}$
09 16 87	-2697026.493	0.007	-10313.601	0.032	-2707340.093	0.032
09 18 87	-2697026.493	0.007	-10313.602	0.037	-2707340.095	0.037
					Mean: -2707340.094	0.036
DATE	FT ORD Y	$\sigma_{ORD\,Y}$	ΔY	$\sigma_{\Delta Y}$	MRY Y	$\sigma_{MRY\,Y}$
09 16 87	-4354393.309	0.010	917.693	0.048	-4353475.617	0.049
09 18 87	-4354393.309	0.010	917.689	0.049	-4353475.620	0.050
					Mean: -4353475.618	0.051
DATE	FT ORD Z	$\sigma_{ORD\,Z}$	ΔZ	$\sigma_{\Delta Z}$	MRY Z	$\sigma_{MRY\,Z}$
09 16 87	3788077.778	0.009	-6337.391	0.041	3781740.387	0.042
09 18 87	3788077.778	0.009	-6337.389	0.044	3781740.389	0.045
					Mean: 3781740.388	0.044

$$\sigma_{C_{MRY}} = \pm \sqrt{\sigma^2_{C_{ORD}} + \sigma^2_{\Delta_c}}$$

where $\sigma_{C_{ORD}}$ is the uncertainty of the Ft Ord coordinate.

One month prior to the surveys originating from Ft Ord, two other surveys were conducted from the satellite Doppler horizontal control point NAVAL POST GRAD 31965 DOPPLER. The Doppler station is approximately 300 m north of the Monterey antenna location (Figure 1). The double differenced GPS carrier phase solutions of the two Doppler-originating surveys yielded the following Monterey coordinates:

X -2707339.725 m

Y -4353475.654 m

Z 3781740.264 m

The baseline components had an uncertainty of ±0.002 m, but the Doppler station has an uncertainty of ±2 m in each coordinate before transformation to WGS84. The results of the Doppler surveys were not used in determining the Monterey coordinates because of the large uncertainty in the Doppler station location. The three-dimensional positions

of the Monterey antenna from the Doppler and the VLBI originating surveys agree to better than 0.5 m.

The two days of pseudorange observations at the Monterey receiver were each subjected to a least-squares estimation and then averaged together to yield the Monterey coordinates:

X -2707334.248 ±1.3 m

Y -4353466.807 ±0.6 m

Z 3781741.330 ±2.2 m

where the two-day standard deviations are given. The deviation of the pseudorange from the differenced carrier phase derived Monterey coordinates is expected because of the coarser resolution of the C A code and because the pseudoranges are corrected for neither tropospheric nor ionospheric delays.

3. Sand Point Coordinates

The Sand Point antenna coordinates were determined by one 90-minute GPS survey (Table 3) from the mobile VLBI site Aviation 2 which is 530 m distant (Figure 1).

Table 3. RESULTS OF SAND POINT ANTENNA LOCATION SURVEY: From double difference carrier phase solutions. Distances and WGS84 Cartesian Coordinates are in meters.

Aviation 2 Coordinate	σ_{AV2}	Δ	σ_{Δ}	Sand Point Coordinate	σ_{SP}
X= -2295347.760	0.017	-408.361	0.002	-2295756.121	0.017
Y= -3638029.429	0.028	330.200	0.002	-3637699.228	0.028
Z= 4693408.964	0.032	73.813	0.003	4693482.777	0.032

The Sand Point antenna coordinates computed from the pseudorange data were:

X -2295749.623 m

Y -3637694.279 m

Z 4693488.472 m

and standard deviations are not given because this is a single observing session and the program does not provide solution standard deviations.

4. Monterey-Sand Point Baseline Components

First the Monterey-Sand Point baseline components were computed by subtracting the Sand Point Cartesian coordinate from the respective Monterey Cartesian coordinate. The uncertainties in the baseline components were computed as the square root of the sum of the squares of the uncertainty of the Monterey and Sand Point coordinates. The slope distance was computed as the square root of the sum of the squares of the baseline components. The slope distance uncertainty was computed as:

$$\sigma_b = \sqrt{(\frac{\Delta X}{b}\sigma_{\Delta X})^2 + (\frac{\Delta Y}{b}\sigma_{\Delta Y})^2 + (\frac{\Delta Z}{b}\sigma_{\Delta Z})^2}$$

where b is the slope distance. Using the information from Tables 2 and 3 gives Table 4, which is used as a standard to estimate accuracy.

Table 4. STANDARD BASELINE DISTANCES AND 2-SIGMA VALUES.

ΔX	-411583.973	± 0.080 m	(0.19 ppm)
ΔY	-715776.390	± 0.116 m	(0.16 ppm)
ΔZ	-911742.388	± 0.109 m	(0.12 ppm)
Slope Distance	1230045.280	± 0.109 m	(0.09 ppm)

C. THE ONE WAY CARRIER BEAT PHASE

The development of the carrier beat phase technique and a model for its application are given by Remondi [1984]. The phase measurement is done by beating the received carrier with a local oscillator internal to the GPS receiver. The slant range from a GPS receiver to a GPS satellite can be modelled in terms of the time it takes the signal to travel or the number of cycles that occur between the satellite and the receiver. The range in cycles will consist of an integer and fractional number of cycles. When a GPS receiver locks onto the carrier signal, it can immediately measure the fractional part and begin counting subsequent integer cycles, but it cannot measure or account for the initial integer number of cycles that preceded the initial fractional part. These missing cycles bias subsequent measurements and are called the initial integer ambiguity biases.

The signal does not take a direct path to the receiver as it is refracted by the ionosphere and troposphere. Additional errors are caused by the satellite deviating from its predicted orbit, errors in the satellite clock, and errors in the receiver clock. Anticipating that the observables will be used in relative positioning, that a single frequency receiver will be used and ignoring other error sources, such as multipath, the one-way

carrier beat phase, $\phi_b(r,s,i)$, observed at receiver, r, from satellite, s, at observation epoch, i, can be modelled to first-order as:

$$\begin{aligned}\phi_b(r,s,i) = \phi_s(i) - \phi_r(r,i) - \frac{f_s}{c}\rho(r,s,i) \\ + \zeta(r,i)\left[f_s + f_r - \frac{f_s}{c}\dot{\rho}(r,s,i)\right] \\ - \tau(r,i) + A(r,s,1)\end{aligned} \tag{2.1}$$

where:

i	Epoch identifier
r	Receiver identifier
s	Satellite identifier
$\phi_s(i)$	Phase of received carrier signal
$\phi_r(r,i)$	Phase of receiver generated carrier signal
f_s	Transmitted frequency of carrier signal
$\rho(r,s,i)$	Satellite-receiver slant range
$\dot{\rho}(r,s,i)$	Time rate of change of slant range
c	Speed of light
f_r	Receiver generated carrier frequency
$\tau(r,i)$	Tropospheric delay
$A(r,s,1)$	Initial integer ambiguity

$$\zeta(1,i) = \xi(i) - \frac{\delta(i)}{2}$$

$$\zeta(2,i) = \xi(i) + \frac{\delta(i)}{2}$$

$\xi(i)$	Mean clock offset for both receivers
$\delta(i)$	Clock drift between both receivers

and parentheses do not indicate factors or functions, but simply enclose identifiers. Brackets indicate factors.

D. DIFFERENCING THE ONE-WAY CARRIER BEAT PHASE

1. Single Difference

The single difference (SD) is formed by differencing carrier beat phase observables from two receivers at the same observation epochs. Following Remondi [1984], taking the difference, expanding the $\zeta(r,i)$ terms of Equation (2.1), and expressing differences in the between-satellite and between-receiver phases as $f_s\delta(i)$ gives:

$$
\begin{aligned}
SD(s,i) &= \phi_b(2,s,i) - \phi_b(1,s,i) \\
&= \frac{f_s}{c}\left[\rho(2,s,i) - \rho(1,s,i)\right] \\
&\quad + \frac{f_s}{c}\left[\dot{\rho}(2,s,i) - \dot{\rho}(1,s,i)\right]\xi(i) \\
&\quad - \left[f_1 - f_2\right]\xi(i) + f_s\delta(i) \\
&\quad + \frac{f_s}{2c}\left[\dot{\rho}(2,s,i) + \dot{\rho}(1,s,i)\right]\delta(i) \\
&\quad + f_s\left[\tau(2,i) - \tau(1,i)\right] + A(2,s,1) - A(1,s,1)
\end{aligned}
\tag{2.2}
$$

where the terms are the same as Equation (2.1). Single differencing reduces or eliminates satellite orbital and clock errors because they are common to both receivers.

2. Double Difference

A double difference (DD) is formed by differencing single differences between a reference satellite, h, and another satellite at the same epoch:

$$DD(h,s,i) = SD(h,i) - SD(s,i)$$

Because the differences at the same epoch are taken with the same reference satellite, the double differences for each epoch are correlated. The advantage of the double differences is that the clock dependent terms - $f_s\delta(i)$ and $\left[f_2 - f_1\right]\xi(i)$ - are eliminated. The significance of the removal of those terms is to reduce from nanoseconds to microseconds the timing accuracy required to achieve one cycle accuracy. The Trimble 4000SX achieves sub-microsecond accuracy by using the C/A code timing information [Ashjaee, 1985].

3. Triple Difference

A triple difference (TD) is formed by differencing the double differences for the same satellite pair at some integer number of succeeding epochs, l :

$$TD(i) = DD(h,s,i + l) - DD(h, s,i)$$

The advantage of the triple difference is that it eliminates all the time independent terms, namely the initial integer ambiguities, $A(r,s,1)$, and becomes insensitive to the initial ambiguities and any cycle slips when the receiver loses lock.

The disadvantages of the triple difference are: another level of correlation, loss of resolution, and reduced number of observations. The triple differences are already correlated with respect to satellite because of the underlying double differences, and are

further correlated with respect to time because consecutive triple differenced observations will have the $DD(h,s,i+1)$ term in common.

For short baselines, integer ambiguities can easily be resolved because unmodelled errors are highly correlated between the two antenna sites and are mostly eliminated by the differencing. Algorithms can take advantage of the integer nature of the initial ambiguities and solve for them. At longer baselines the unmodelled errors are not as highly correlated and not eliminated by the differencing. These errors fold into the initial ambiguities, so that the ambiguities are no longer integers. In some cases the ambiguities cannot be resolved (*e.g.*, Henson and Collier, 1986, Tables 1 and 2).

Because of the advantages the triple difference offers for long baselines, I use the triple difference scheme. While the triple difference can be decorrelated by forming a weight matrix [Remondi, 1984], only the correlated triple difference software was available to me.

E. ERROR EFFECTS

For long baseline GPS surveys, the primary errors are satellite orbit errors, ionospheric and tropospheric delays [Remondi, 1984, and Beutler *et al.*, 1986]. Orbit (ephemeris) errors are the result of the departure of the satellite from the broadcast ephemeris orbit. The ephemeris is a *predicted* orbit for the satellite. Orbit errors propagate directly into the baseline measurements when the GPS orbit coordinates are fixed in the processing [Hothem and Williams, 1985]. Orbit errors can be the dominant error source affecting the repeatability of long baseline measurements [Lichten and Border, 1987].

The magnitudes of baseline errors increase with increasing baseline length because of the increasing projection of the ephemeris error onto the baseline component [Fell, 1980]. Estimates of the broadcast ephemeris error range from 25 m [Beutler *et al.*, 1986] to 100 m [Wells *et al.*, 1986]. The magnitude of the effect of the ephemeris error on baseline accuracy has been traditionally approximated [Beutler *et al.*, 1984, Equation (2.1)]:

$$\frac{E_b}{b} \simeq \frac{E_\rho}{\rho} \tag{2.3}$$

where:

- b baseline length
- ρ slant range (receiver to satellite)

E_b error in baseline length

E_ρ error in slant range

The slant range to a GPS satellite is about 20,000 km, which translates to a baseline error ranging from 1 ppm to 4 ppm using Equation (2.3).

It is expected that the ephemeris error for the Monterey-Sand Point baseline will be towards the lower end of the range because the ephemerides are uploaded prior to the satellites entering the Yuma Proving Ground [Russell and Schaibly, 1980] near the California border. The ephemeris linearization error specification is to 1 m per day [Wells *et al.*, 1986].

The ionosphere disperses the code (the group velocity) from the carrier phase (phase velocity) because the C/A code has a frequency of 1 MHz while the carrier signal upon which it is superimposed has a frequency of 1575 MHz. The effect is to increase the pseudoranges, but decrease the carrier phase derived ranges [Smith, 1987]. Field experiments [Beutler *et al.*, 1986] showed that ionospheric dispersion shortens baselines on the order of a few tenths to perhaps 2 ppm.

Ionospheric error is proportional to the Total Electron Content (TEC) along the signal path and the cosecant of the elevation angle of the satellite [Smith, 1987]. Thus the error is greatest for low elevation angles and least at the zenith. Wells *et al.* [1986] estimated that the range errors due to the ionosphere are from 150 m at the horizon to 50 m at the zenith.

Ionospheric activity is a function of latitude, longitude, time of day, season, and sunspot activity. Ionospheric activity increases towards the equator and towards the sunlit portions of the earth. Diurnally, it has a minimum near 0600 local time with a maximum around 1600 local. Ionospheric activity increases with the peak in the sunspot cycle. The minimum in the current 11-year sunspot cycle occurred in 1986. Upon these systematic characteristics sporadic ionospheric disturbances are superimposed.[Henson and Collier, 1986]

The tropospheric error is proportional to the refractivity along the satellite-receiver path and proportional to the cosecant of the elevation angle [Martin, 1980]. The index of refraction, n, is the ratio of the speed of light in a vacuum to the speed of light in a particular medium, in this case the troposphere. Because the refractive index is a small fraction greater than 1.0, a more convenient unit to work with is refractivity, N, where $N = (n - 1) \times 10^6$. The magnitude of the tropospheric biases range from 20 m for 10° elevation angles to 2.3 m at the zenith [Wells *et al.*, 1986].

Henson and Collier [1986] have shown that triple difference measurements are unaffected by path-dependent ionospheric bias errors, but by path-dependent gradient ionospheric errors, and Martin [1980] has estimated that the ***combined*** ionospheric and tropospheric gradient errors are on the order of meters per hour and are proportional to the cosecant of the elevation angle.

III. DATA COLLECTION, PROCESSING, AND ANALYSIS

A. EQUIPMENT CONFIGURATION

1. Hardware

A complete description of the Trimble 4000SX receiver is given by Trimble Navigation [1987a]. NPS operates three Trimble 4000SX GPS Surveyor receivers, of which two were used in this study. The 4000SX is capable of observing the C/A code, integrated Doppler and carrier beat phases of up to five satellites simultaneously. Its ability to use the C/A code allows the receiver to be used as a stand alone navigation system which determines position using Doppler-smoothed pseudoranges and velocities [Ashjaee, 1985].

For precise relative positioning the 4000SX can transmit its data through an RS232 port to a microcomputer for storage on floppy disk for post-processing. The 4000SX's ability to use the C/A code allows it to decode the GPS navigation messages so that it can track satellites automatically and determine. Most importantly, it uses the C/A code in a time transfer mode to determine any offset and drift of its own clock and thus provide accurate time tags for the observations without an external atomic clock or synchronization with the receiver at the other end of the baseline.

The receivers were left on continuously to allow unattended data collection.

Multipath-resistant Trimble microstrip antennas were installed at both the Monterey and Sand Point locations.

2. Software

For relative positioning, the receiver is controlled from the microcomputer by Version D of Trimble's *Datalogger* program. The reference position (the geodetic coordinates of the antenna) and the particular options chosen must be entered into the receiver via the receiver keypad. The receivers were set to use the reference position height for point positioning when less than four satellites were available.

Each observation session was initialized to log data when a minimum of four satellites were 15° above the antenna's horizon. Five satellites were designated for each observing session. The software logs the observables and receiver clock parameters to a floppy disk every 15 seconds and the C/A code-determined antenna position and Position Dilution of Precision (PDOP) every five minutes. The GPS navigation message is logged to a separate file at the beginning of the session.

B. SATELLITE OBSERVATION PLAN

1. Satellite Selection

The same five satellite (SV) (6, 9, 11, 12, and 13) were used for the entire eight-week observation period. These five satellites were visible at both stations for over 100 minutes, and of these five satellites four were visible for three hours (Figure 2).

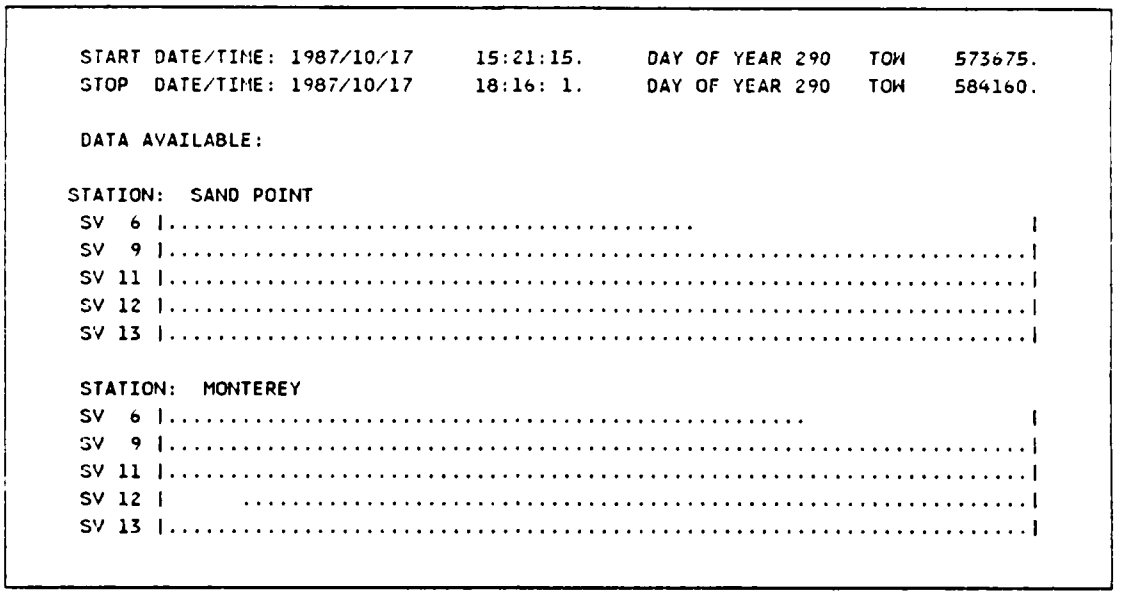

Figure 2. Satellite availability: Each dot represents 10 observations; each column, 10 epochs. From *Trim640* output.

2. Position Dilution of Precision (PDOP)

Trimble Navigation [1987b] recommends that observations include the time that the PDOP goes to infinity. The Federal Geodetic Control Committee [1986] notes that initial results from investigations indicate that best results may be achieved when the Geometric Dilution Of Precision (GDOP) is changing value during the observing session, and proposes that observing sessions start with a high GDOP and stop with a low GDOP.

Position Dilution of Precision is a component of the GDOP. GDOP is a measure of how satellite geometry degrades point position accuracy [Jorgensen, 1984]. For computational ease in the navigation solution the GDOP is defined as the square root of the trace of the covariance matrix of the errors in ***position*** and time with the range errors set to one [Milliken and Zoller, 1980]. The rôle and definition of GDOP and PDOP in GPS point positioning were applied to GPS relative positioning, *i.e.*, good

PDOP would provide better accuracy than poor PDOP [King *et al.* 1985]. Good and poor PDOP are shown in Figure 3.

Landau and Eissfeller [1986], using numerical simulations in which they assumed a full 18 satellite constellation and a receiver that could track those satellites that minimized GDOP, found that better accuracy for triple difference solution for a 68 km baseline generally corresponded to high GDOP. They used a more complete GDOP that included consideration of ionospheric, tropospheric and satellite position errors which are neglected in the conventional GDOP.

The 4000SX does not record GDOP, but it does record PDOP every five minutes. PDOP relates to GDOP as: $GDOP^2 = PDOP^2 + TDOP^2$, where TDOP is the Time Dilution Of Precision, the error in the user clock bias multiplied by the velocity of light. The expected uncertainty in a GPS point positioning solution is a product of the PDOP and the expected slant range error. The difference between PDOP's at Monterey and Sand Point remained less than 1.0 for the entire eight week observing period. The PDOP peaks at two times in an observing session (Figure 4) - 60 minutes and 150 minutes. The PDOP peaks occur near when the satellites lie in a common plane causing the solution of the linearized range equations to diverge and the PDOP becomes infinite [Jorgensen, 1984].

C. METEOROLOGICAL PARAMETERS

Meteorological parameters are needed for the tropospheric correction model used in the processing software. On-site meteorological observations were not available for Sand Point. Instead observations from the Weather Service Office (WSO) of the Seattle-Tacoma International Airport (SEA-TAC) were used for Sand Point. SEA-TAC is approximately 27 km from Sand Point (Figure 1). The NPS Department of Meteorology routinely collects real-time hourly observations of sea-level pressure, temperature and relative humidity from the National Weather Service's data network. Observations that pertained to GPS observing sessions were entered into a file that is accessed by the batch file building program.

While the Federal Geodetic Control Committee [1986] has proposed the use of on-site meteorological parameters, researchers have had success using standard atmosphere parameters for satellite geodesy [Fell, 1976] or extrapolated meteorological data [Rathacher *et al.*, 1986].

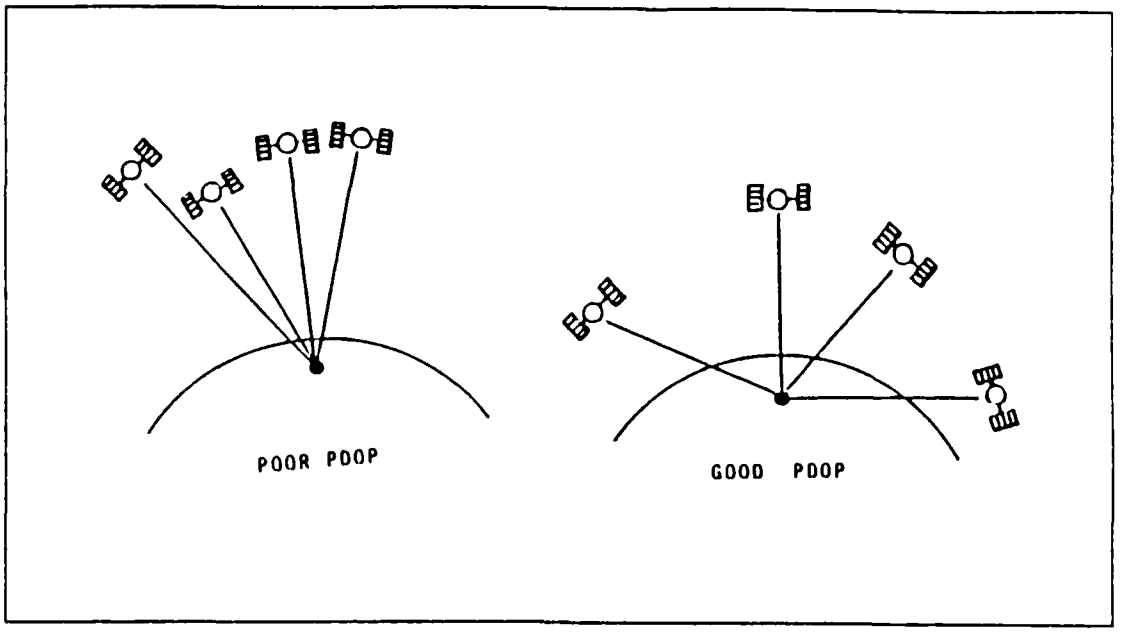

Figure 3. Poor and good PDOP: From King *et al.* [1985, Fig. 3.2].

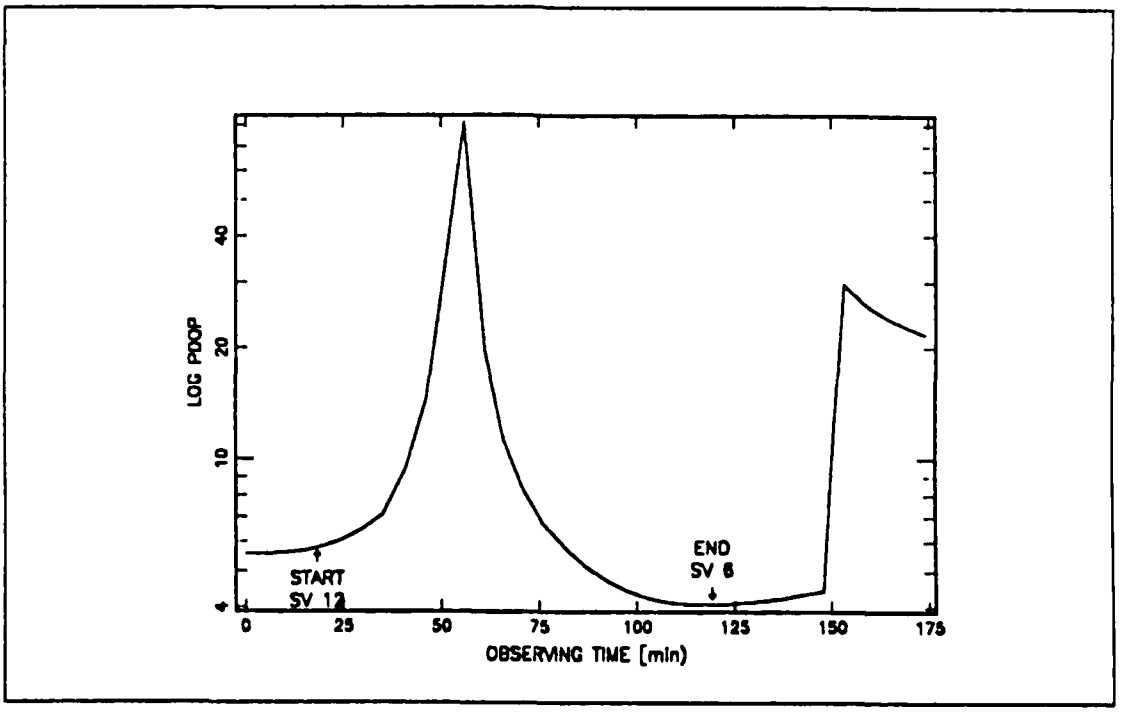

Figure 4. PDOP versus time

Hourly observations for Monterey were obtained from the NPS Department of Meteorology. The instruments were located approximately 300 m south of the Monterey antenna location (Figure 1).

D. PROCESSING SOFTWARE

A complete description of the Trimble supplied *Trimvec* software can be found in Trimble Navigation [1987b]. The data was processed using the *Trimvec Trim640* program, Revision AB. *Trim640* limits processing to 700 epochs, so the first 700 epochs for each observing session are used. Sand Point was used as the reference station and its coordinates kept fixed in the least-squares processing. Sand Point was chosen as the reference station because four satellite availability occurred later at Sand Point than at Monterey. This avoided having to load the not-in-common epochs from Monterey at each processing.

Trim640 uses the C A code derived positions obtained at the lowest PDOP for the initial estimates of the baseline components. *Trim640* culls the best C A code position during the data loading. No ionospheric correction is provided by the software, and only the broadcast ephemeris can be used to compute fixed orbit satellite positions. In the triple difference processing, the only parameters estimated by the least-squares processing are the baseline components, ΔX, ΔY and ΔZ.

A modified Hopfield tropospheric model [Goad and Goodman, 1974] is used to correct the carrier phase delay caused by the troposphere. The correction is a function of the atmospheric refractivity computed from surface meteorological values of pressure, temperature, and humidity, and the elevation angle of the satellite. Larger corrections are required for low elevation angles, as the signal travels a longer path through the troposphere. The model corrects for at least 90% of the tropospheric delay [Remondi, 1983]. *Trim640* allows only one pressure, temperature and humidity entry for each site per session.

E. PROCESSING PROCEDURES

1. General

To study optimized times, the data from each observing session were segmented. Each successive segment contained 10 minutes more data than its predecessor. For example, for an entire observing session that started when four satellites were available and stopped when less than four were available provides 175 minutes of observations. The first segment will use the first 10 minutes of data , the sixth segment will use the first 60 minutes, while the eighteenth will use all 175 minutes. For each segment, the entire

processing was restarted from the data loading. Reloading the data for each segment takes considerably longer than using the *Trim640* option to flag data for processing, but reloading was done so that the processing does not use a best C A code position from later in the observing session.

Convergence of the least-squares solution was achieved by doing five iterations using every tenth triple difference formed from every tenth double difference, followed by five iterations decreasing the triple and double difference increments to five, and finally five iterations using all triple differences formed from all double differences.

Trim640 rejects those observations whose residuals exceed a multiple of the mean residual. The multiple of the mean residual is known as the *edit multiplier*. *Trim640* uses 3.5 as the default value for the edit multiplier. I used the default value for the initial processing.

Any segment that had more than ten percent of its observations rejected or whose solution slope distance standard deviation (σ_s) was greater than 10 m was reprocessed. The reprocessing was identical to the initial processing except that before invoking the triple difference process the pseudoranges for both stations were subjected to separate least-squares adjustment. The pseudorange processing improves the C A code derived initial estimates for the baseline components and corrects the carrier beat phase time tags. The carrier beat phase time tags are computed from the C A code times, and are earlier than the C A code times.

If the pseudorange processing failed to lower the rejections to ten percent, the edit multiplier was increased until the rejections reached ten percent. A ten percent rejection level was observed for a few sessions and always occurred within the first thirty minutes of observations. The data were transferred to the Naval Postgraduate School's IBM 3033 computer for analysis. The data were analysed and graphics produced using the *APL*-based *GRAFSTAT* program.

To study the effects of reducing observation time, five case studies were undertaken in which the observation start times were changed for processing. Each case study followed the processing procedures outlined above.

2. Batch Processing

Processing is performed in a batch mode. A batch file passes parameters to a template. Trimble supplies command files that tell the *Trim640* to use the template parameters in processing.

The batch file is built using the program *Bathld* (Appendix A). *Bathld* builds a batch file by providing the appropriate file names and start and stop times. *Bathld* computes the appropriate meteorological parameters for each segment by locating the applicable weather observations from the weather observation file, interpolating values at the start time, computing running means from each hourly weather observation, then interpolating the running means to the stop time of each segment. Two millibars were subtracted from the SEA-TAC sea-level pressure to compensate for the 20-m elevation above sea-level for the Sand Point antenna.

Initially, processing was done on an IBM XT with a math coprocessor and a hard disk. Processing the 18 segments of an observing session took ten hours of computing time. Later, processing was performed on an 80286 based microcomputer running at 10 MHz with an 80287-8 math coprocessor that reduced the processing time to three hours.

Two minor problems with *Trim640* were discovered during the processing. First, large values in range differences were found when using the range differences rather than the pseudoranges to improve the C A code positions. The data were forwarded to Trimble Navigation for evaluation and an error was found in their software. The error had no apparent effect upon carrier phase difference processing. Second, *Trim640* is incompatible with one or more of the AST Research, Inc. device drivers supplied with the 80286 microcomputer: ram disk, print spooler, and extended memory. Removing the drivers allowed *Trim640* to execute normally.

At the conclusion of the batch processing, the slope distance, the baseline components, their standard deviations (σ_i), the number of observations, the number of observations rejected, and the RMS cycle fits were extracted from the *Trim640* output file and collected into files that held the data for a particular segment for each case study.

F. ANALYSIS PARAMETERS

The statistical parameters that will be used to evaluate the results are the error, the sample mean and the standard deviation defined as [Davis *et al* ., 1981]:

$$E_d = C_d - C_S \tag{5.1}$$

$$\overline{E} = \frac{1}{m}\sum_{d=1}^{m} E_d$$

$$\sigma^2 = \frac{1}{m-1} \sum_{d=1}^{m} (E_d - \bar{E})^2$$

$$\sigma_{\bar{E}} = \frac{\sigma}{\sqrt{m}} \tag{5.2}$$

where:

E_d Error for day d

C_d Measured component for day d

C_S Expected values

$\bar{E}$ Mean error or bias

σ^2 Variance

σ Standard deviation of E_d

$\sigma_{\bar{E}}$ Standard deviation of $\bar{E}$

Accuracy describes the closeness between the measurements and the *expected* values [Davis *et al.*, 1981]. The degree of accuracy is determined to the magnitude of the mean error ($\bar{E}$). The repeatability of the measurements will be expressed in terms of 2σ because it approximates the 95% confidence level for single-dimension measurements [Federal Geodetic Control Committee, 1986]. The slope distance and individual baseline components are one-dimensional measurements.

G. DATA AVAILABILITY

Observations were made simultaneously at Monterey and Sand Point for an eight-week period beginning 29 September 1987. Observations were made Tuesday through Saturday except the days after federal holidays. Forty observing sessions were conducted of which 28 were used in the analysis and are listed in Table 5. The remaining 12 days of observations were not used in the analysis for various reasons, which are listed in Table 6.

For brevity the observing days will be referred to by their Julian day. Times in Table 5 are given in Pacific Standard Time (PST) rather than Universal Coordinated Time (UTC) for ease in the later discussions on diurnal effects.

Table 5. DAYS USED IN THE DATA ANALYSIS

Date	Julian Day	Start Time (PST)	End Time (PST)	Number of Triple Difference Observations
09 29 87	272	0833	1129	1599
09 30 87	273	0830	1125	1485
10 01 87	274	0825	1121	1501
10 02 87	275	0822	1118	1479
10 03 87	276	0817	1113	1518
10 06 87	279	0805	1100	1563
10 07 87	280	0801	1056	1490
10 08 87	281	0757	1053	1508
10 09 87	282	0753	1049	1500
10 10 87	283	0749	1044	1522
10 14 87	287	0732	1028	1524
10 17 87	290	0721	1016	1504
10 20 87	293	0707	1002	1540
10 21 87	294	0703	0958	1562
10 22 87	295	0658	0953	1551
10 24 87	297	0651	0946	1493
10 27 87	300	0638	0934	1567
10 28 87	301	0634	0930	1516
10 29 87	302	0631	0926	1681
11 03 87	307	0613	0908	1848
11 04 87	308	0605	0901	1553
11 05 87	309	0601	0857	1695
11 10 87	314	0541	0837	1535
11 11 87	315	0536	0832	1927
11 13 87	317	0528	0824	1923
11 14 87	318	0524	0819	1550
11 21 87	325	0455	0750	1595
11 25 87	329	0438	0734	1854

Table 6. OBSERVATION DAYS NOT USED IN THE ANALYSIS.

Date	Reason for not analyzing
10 15 87	No SEA-TAC weather observations
10 16 87	No satellites at Monterey for first 10 minutes
10 23 87	Slope distance σ, > 10 m for first 10 minutes
10 30 87	Disk error
10 31 87	No SEA-TAC weather observations
11 06 87	Unhealthy satellites
11 07 87	Unhealthy satellites
11 17 87	Unhealthy satellites
11 18 87	Unhealthy satellites
11 19 87	Unhealthy satellites
11 20 87	Unhealthy satellites
11 24 87	No satellites at Monterey for first 20 minutes

Day 283 was processed with Monterey as the fixed reference station because the data set would not partition into 10-minute segments when Sand Point was used as the reference station.

The days that were missing one or two segments were excluded from the analysis, so that changes in the sample variances would not be due to unequal sample populations between the segments.

Reprocessing the first segment for 23 October failed to reduce the slope distance sigma to less than 10 m because that segment had only nine triple difference observations because the receiver frequently lost lock on the satellites. That day was not used in the analysis, even though its other segments had slope distance sigma's less than 10 m without reprocessing.

IV. RESULTS AND DISCUSSION

A. GENERAL

To study optimized times, five cases are studied:

1. Process all data when four satellites at least 15° above horizon
2. Begin processing when five satellites at least 15° above the horizon
3. Begin processing as in 2, but delete fifth satellite
4. Begin processing data 40 minutes later than in 1
5. Begin processing data 70 minutes later than in 1

Case 1 is essentially the processing of the full data set. Each of the other cases is a subset of Case 1. *Trim640* allows the user to designate at what time within the full observing period that the data loading should begin. For Case 3, *Trim640*'s ability to flag data was used to exclude the fifth satellite (SV 12) from the processing. Each day of Table 5 was processed for each of the five cases.

During the course of the discussions it will be necessary to distinguish between observation periods and the time of the observations fixed with respect to satellite geometry. As the satellite geometry (PDOP) begins with the availability of four satellites, the time of observations can be defined in terms of the Case 1 start time. Observation periods are determined from the start time for each case. Times of observations will given as equivalent Case 1 times and is obtained by adding the case observation length to the case's time offset from Case 1 (Case 2 and 3's offsets are 20 minutes; Case 4, 40 minutes and Case 5, 70 minutes).

B. ACCURACY

1. Slope Distance

The slope distance errors for Cases 1, 2, 4, and 5 are presented in Table 7. Then results show that accuracy to better than 1.0 ppm is achieved for any observation period, but that there are differences among the cases and with changing observation periods within each case.

Cases 1, 2, and 4 exhibit similar behavior as the observation period increases - they become less positive (or more negative) as the observation period increases until they reach a minimum, then they reverse their trends and become less negative. Positive error indicates that the measured baseline is longer than the standard values, so that the

measured baselines are exhibiting an *accordion* effect as they shorten then lengthen as more observations are included in the solutions. While the minimum occurs after different observing periods (140, 110, 90 minutes for Cases 1, 2, and 4 respectively), they occur at about the same absolute time with respect to the Case 1 start time (140, 130, and 130 minutes for Cases 1,2, and 4 respectively). As the start times occur later with each case, the errors for shorter observing periods become less positive and the ranges of the errors for each case decrease (the range of Case 1 errors is +3σ to -18.4 cm; +7.8 to -18.1 cm, for Case 2; and -10.3 to -15.1 cm, for Case 4). The error after the entire observation session decreases with later observing start times (-14.8 cm, -9.1 cm, and -0.4 cm for Cases 1, 2, and 4 respectively).

Case 5 behaves similarly to the previous cases except that its minimum occurs after only 10 minutes of observations and adding more observations causes the error to become positive. The error is largest after the entire observing session (38.4 cm). Cases 1, 2, and 4 start their observations prior to the first PDOP peak that occurs at 60 minutes (Figure 4) while Case 5 starts after the PDOP peak, so that starting the observations close to the larger PDOP peak and including the PDOP peak observations can reduce the error and the required observation period. The effect of the PDOP peak upon the mean slope distance error is readily apparent in comparing Cases 4 and 5. Case 4 remains negative without the early positive error, and Case 5 remains positive as it lacks most of the observations from about the *first PDOP* peak.

The first PDOP peak at 60 minutes differs from the second PDOP peak in that it has a higher value, is symmetric, and occurs farther from the four satellite observation start time than the second peak is from the four satellite observation stop time, *i.e.*, the second peak occurs with lower elevation angles than the first which implies larger tropospheric and ionospheric errors.

The results for Case 3 (excluding the fifth satellite) slope distance errors are presented in Table 8. Case 3 was studied because the Case 2 results showed a decrease in the initial slope distance errors, and Case 3 was to study the effects of observing five satellites. The results show that using only four satellites makes a difference of only a few centimeters from the results using all available satellites. It should be noted that Case 3 uses only three satellites once SV 6 sets after 100 minutes of observations. The Case 3 minimum, -11.5 cm, was less negative than the Case 2 minimum of -18.1 cm.

Table 7. MEAN SLOPE DISTANCE ERROR FOR CASES 1, 2, 4, AND 5

Observation Period [min]	Case 1		Case 2		Case 4		Case 5	
	cm	ppm	cm	ppm	cm	ppm	cm	ppm
10	36.0	0.29	7.8	0.06	-10.3	-0.08	-2.3	-0.02
20	30.4	0.25	2.5	0.20	-10.9	-0.09	5.7	0.05
30	21.7	0.18	-0.4	-0.00	-12.2	-0.10	19.2	0.16
40	15.1	0.12	-3.3	-0.03	-13.0	-0.11	19.7	0.16
50	9.8	0.08	-6.0	-0.05	-12.9	-0.11	17.7	0.14
60	5.3	0.04	-8.6	-0.07	-10.9	-0.09	17.9	0.15
70	0.8	0.01	-10.4	-0.08	-13.2	-0.11	20.6	0.17
80	-3.0	-0.02	-10.7	-0.09	-15.0	-0.12	23.2	0.19
90	-6.0	-0.05	-14.2	-0.12	-15.1	-0.12	27.2	0.22
100	-7.8	-0.06	-16.8	-0.14	-13.4	-0.11	31.7	0.26
110	-12.1	-0.10	-18.1	-0.14	-11.2	-0.09	38.4	0.31
120	-15.9	-0.13	-17.2	-0.14	-8.0	-0.07	-	-
130	-18.1	-0.15	-16.0	-0.13	-4.8	-0.04	-	-
140	-18.4	-0.15	-14.0	-0.11	-0.4	-0.00	-	-
150	-18.0	-0.15	-11.7	-0.10	-	-	-	-
160	-17.0	-0.14	-9.1	-0.07	-	-	-	-
170	-15.6	-0.13	-	-	-	-	-	-
175	-14.8	-0.12	-	-	-	-	-	-

Table 8. CASE 3 MEAN ERRORS

Observation Period [min]	Slope Distance		ΔX		ΔY		ΔZ	
	cm	ppm	cm	ppm	cm	ppm	cm	ppm
10	8.8	0.07	-287.0	-6.97	177.6	2.48	-21.7	-0.24
20	3.7	0.03	-247.0	-6.00	155.5	2.17	-15.6	-0.17
30	-0.4	-0.00	-214.3	-5.21	126.3	1.76	-1.9	-0.02
40	-4.6	-0.04	-199.4	-4.84	110.4	1.54	9.5	0.10
50	-8.5	-0.07	-170.6	-4.15	87.6	1.22	19.7	0.22
60	-10.9	-0.09	-142.2	-3.44	64.9	0.91	27.9	0.30
70	-11.5	-0.10	-115.7	-2.82	44.8	0.63	32.6	0.36
80	-10.1	-0.08	-90.4	-2.19	24.5	0.34	35.1	0.38
90	-10.3	-0.08	-58.7	-1.43	7.2	0.10	34.7	0.38
100	-10.0	-0.08	-38.5	-0.95	9.2	0.13	23.7	0.26
110	-10.3	-0.08	-15.8	-0.39	3.9	0.05	18.0	0.20
120	-10.2	-0.08	5.9	0.15	-1.0	-0.01	11.8	0.13
130	-9.7	-0.08	28.7	0.70	-7.3	-0.10	5.9	0.06
140	-8.8	-0.07	52.9	1.29	-18.6	-0.26	2.5	0.03
150	-7.5	-0.06	73.7	1.80	-29.8	-0.42	0.3	0.00
160	-5.2	-0.04	97.2	2.36	-45.0	-0.63	-1.5	-0.02

2. Baseline Components

The ΔX and ΔY accuracies are better than 10.0 ppm for all observing periods while ΔZ accuracy is better than 1.0 ppm for all observing periods. The accuracy of the baseline components is expected to be less than the accuracy of the baseline because the baseline errors are mostly perpendicular to the baseline itself [Remondi, 1984]. The baseline component results (Tables 9, 10, and 11) show that the ΔX and ΔY errors are greater than the baseline components while the ΔZ errors are about the same order of magnitude as the slope distance errors. The ΔX and ΔY errors are negatively correlated which is the result of the correlations of the triple differences and the semi-circular tracks of the satellites (Figure 5). Case 3 (Table 8) shows little difference from Case 2 in the ΔX error, and a more negative ΔY error is offset by a less negative ΔZ error.

The smallest mean errors for the baseline components are found at various observing periods. Zero mean error for all the baseline components is achieved with fewer observations as the observing start times occur closer to and before the larger PDOP peak.

Table 9. MEAN ΔX ERROR FOR CASES 1, 2, 4, AND 5

Observation Period [min]	Case 1		Case 2		Case 4		Case 5	
	cm	ppm	cm	ppm	cm	ppm	cm	ppm
10	-252.4	-6.13	-296.3	-7.19	-136.3	-3.30	29.6	0.73
20	-255.4	-6.21	-256.0	-6.22	-136.4	-3.30	83.9	2.04
30	-255.5	-6.21	-212.1	-5.15	-107.6	-2.62	132.9	3.23
40	-238.0	-5.78	-194.8	-4.74	-80.1	-1.94	183.9	4.47
50	-211.2	-5.12	-167.8	-4.08	-52.7	-1.29	191.7	4.66
60	-197.0	-4.79	-137.4	-3.33	-24.8	-0.61	192.9	4.69
70	-171.8	-4.17	-107.3	-2.60	21.9	0.53	193.4	4.70
80	-145.1	-3.52	-76.8	-1.87	48.4	1.17	195.4	4.75
90	-116.9	-2.84	-31.8	-0.78	67.7	1.65	201.7	4.91
100	-87.3	-2.11	3.1	0.08	82.3	1.99	208.7	5.08
110	-45.2	-1.09	28.4	0.70	96.2	2.33	221.0	5.37
120	-10.7	-0.27	48.6	1.18	112.0	2.72	-	-
130	15.2	0.36	65.7	1.60	124.8	3.04	-	-
140	35.6	0.87	83.3	2.02	139.9	3.40	-	-
150	53.6	1.30	97.7	2.37	-	-	-	-
160	70.7	1.72	110.1	2.67	-	-	-	-
170	84.3	2.04	-	-	-	-	-	-
175	91.7	2.24	-	-	-	-	-	-

Table 10. MEAN ΔY ERROR FOR CASES 1, 2, 4, AND 5

Observation Period [min]	Case 1		Case 2		Case 4		Case 5	
	cm	ppm	cm	ppm	cm	ppm	cm	ppm
10	188.0	2.63	199.2	2.78	110.0	1.54	9.1	0.13
20	181.2	2.53	181.4	2.53	106.3	1.49	-28.0	-0.39
30	179.3	2.50	152.4	2.13	93.6	1.31	-68.6	-0.96
40	171.2	2.39	139.3	1.95	79.8	1.11	-95.2	-1.33
50	153.0	2.14	125.3	1.75	66.6	0.93	-92.6	-1.29
60	141.0	1.97	109.5	1.53	52.2	0.73	-91.9	-1.28
70	127.7	1.78	94.3	1.32	29.3	0.41	-89.7	-1.25
80	114.0	1.59	79.3	1.11	21.6	0.30	-89.3	-1.25
90	100.5	1.40	58.4	0.82	11.1	0.16	-95.6	-1.33
100	86.4	1.21	46.4	0.65	4.0	0.06	-105.4	-1.47
110	66.7	0.93	34.0	0.47	-3.3	-0.05	-121.0	-1.69
120	55.8	0.78	23.5	0.33	-15.8	-0.22	-	-
130	43.3	0.60	14.8	0.21	-27.7	-0.39	-	-
140	33.9	0.47	2.9	0.04	-42.5	-0.59	-	-
150	25.5	0.36	-9.0	-0.13	-	-	-	-
160	14.4	0.20	-17.0	-0.24	-	-	-	-
170	4.0	0.06	-	-	-	-	-	-
175	-1.8	-0.03	-	-	-	-	-	-

Table 11. MEAN ΔZ ERROR FOR CASES 1, 2, 4, AND 5

Observation Period [min]	Case 1		Case 2		Case 4		Case 5	
	cm	ppm	cm	ppm	cm	ppm	cm	ppm
10	-82.2	-0.90	-33.2	-03.6	-11.0	-0.12	-17.4	-0.19
20	-68.0	-0.75	-30.2	-0.33	-7.3	-0.08	-23.6	-0.26
30	-54.8	-0.60	-23.4	-0.36	-8.5	-0.09	-32.0	-0.36
40	-47.3	-0.52	-17.0	-0.19	-8.9	-0.10	-34.8	-0.38
50	-38.1	-0.42	-14.6	-0.16	-11.1	-0.12	-37.7	-0.41
60	-28.9	-0.32	-12.3	-0.13	-15.1	-0.17	-39.1	-0.42
70	-23.8	-0.26	-11.6	-0.13	-15.1	-0.17	-44.7	-0.49
80	-20.0	-0.22	-13.1	-0.14	-18.5	-0.20	-49.5	-0.54
90	-18.1	-0.20	-12.4	-0.14	-18.9	-0.20	-52.7	-0.58
100	-17.9	-0.20	-15.1	-0.17	-22.2	-0.24	-54.2	-0.59
110	-15.6	-0.17	-15.1	-0.17	-25.7	-0.28	-56.5	-0.62
120	-17.5	-0.19	-17.2	-0.19	-27.3	-0.30	-	-
130	-16.4	-0.18	-19.8	-0.22	-28.0	-0.31	-	-
140	-17.9	-0.20	-21.0	-0.23	-29.3	-0.32	-	-
150	-19.9	-0.22	-21.3	-0.23	-	-	-	-
160	-20.3	-0.22	-21.9	-0.24	-	-	-	-
170	-20.1	-0.22	-	-	-	-	-	-
175	-20.1	-0.22	-	-	-	-	-	-

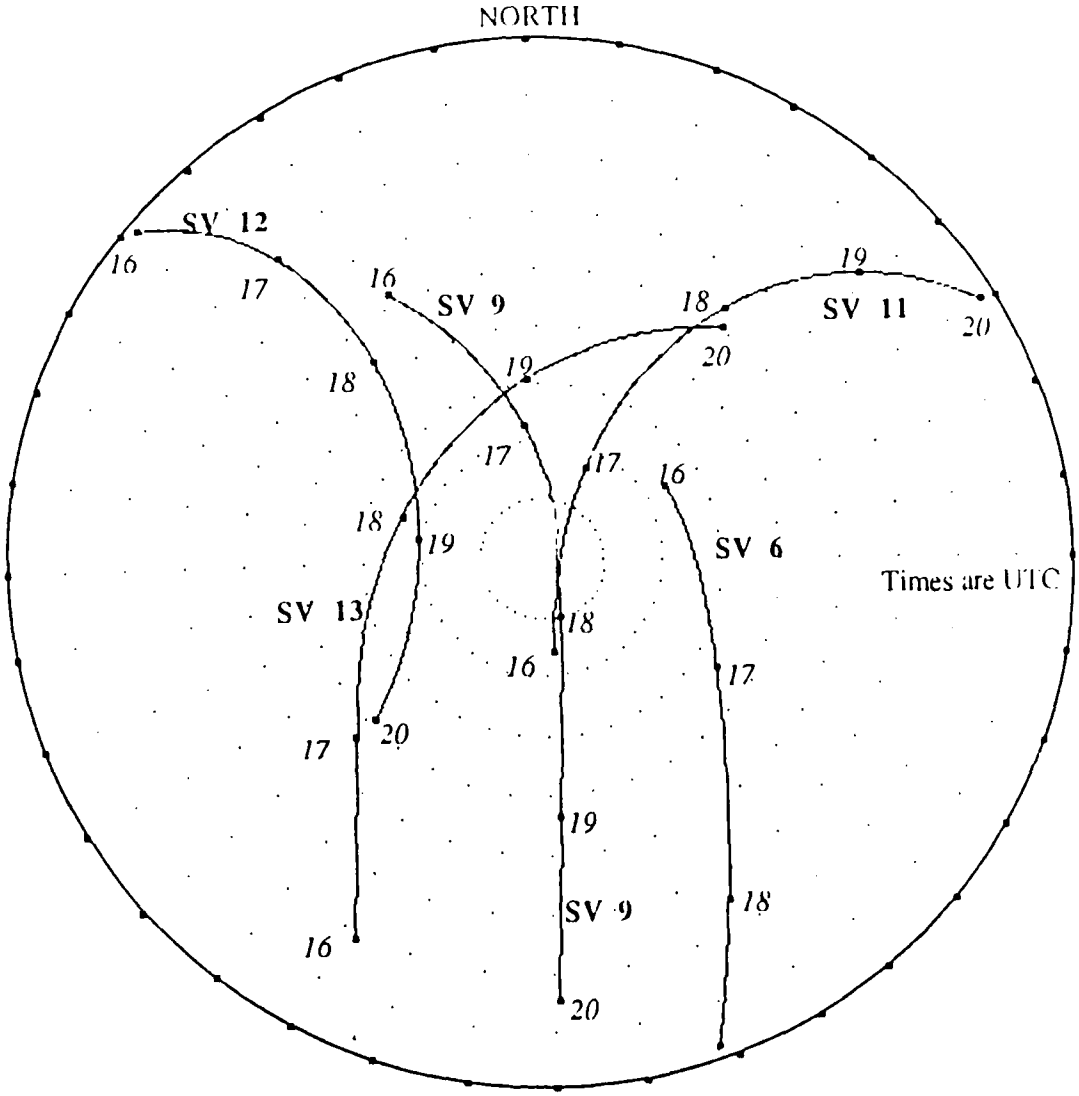

Figure 5. Sky Plots of satellite tracks for Monterey: Elevation angles are dotted concentric circles. Zenith is at the center.

C. REPEATABILITY

1. Slope Distance

The day-to-day repeatabilities, represented as the 2σ level, for Cases 1, 2, 4, and 5 are presented in Table 12, and for Case 3, in Table 13. All the cases achieve 1.0 ppm repeatability for any observing period except Case 1 which requires 20 minutes of observations. Repeatability eventually reaches better than 0.5 ppm after 60 minutes of observations for any case.

The minimum 2σ levels for all cases are reached at the 80 to 90 minute time of observation, which is about 30 minutes after the larger PDOP peak. A slight increase in the 2σ level is centered about the 120 to 130 minute time of observation for all cases which is near the PDOP minimum, after which the 2σ level decreases slightly as observations from the second PDOP peak are included in the solutions. Case 4 had the narrowest range of 2σ values, and Case 1 had the widest range of 2σ values.

Table 12. SLOPE DISTANCE 2-SIGMA VALUES FOR CASES 1, 2, 4, AND 5

Observation Period [min]	Case 1		Case 2		Case 4		Case 5	
	cm	ppm	cm	ppm	cm	ppm	cm	ppm
10	176.8	1.44	64.8	0.53	57.8	0.47	52.0	0.42
20	118.2	0.96	63.2	0.51	56.8	0.46	53.4	0.43
30	84.1	0.68	58.6	0.48	59.2	0.48	60.8	0.49
40	69.8	0.57	58.4	0.47	53.8	0.44	57.0	0.46
50	64.0	0.52	58.6	0.48	54.4	0.44	55.4	0.45
60	61.8	0.50	55.2	0.45	57.6	0.47	55.0	0.45
70	60.4	0.49	55.0	0.44	59.6	0.48	53.6	0.44
80	57.4	0.47	56.8	0.46	60.4	0.49	53.6	0.44
90	56.2	0.46	59.0	0.48	60.8	0.49	57.6	0.46
100	57.2	0.47	60.0	0.49	59.6	0.48	62.6	0.51
110	59.2	0.48	60.4	0.49	57.8	0.47	67.8	0.55
120	60.0	0.49	59.6	0.48	56.2	0.46	-	-
130	61.0	0.50	59.0	0.48	56.0	0.46	-	-
140	60.6	0.49	58.2	0.47	55.4	0.45	-	-
150	60.0	0.49	57.8	-	-	-	-	-
160	59.0	0.48	58.4	-	-	-	-	-
170	58.6	0.48	-		-	-	-	-
175	58.6	0.48	-		-	-	-	-

Table 13. CASE 3: 2-SIGMA VALUES

Observation Period [min]	Slope Distance		ΔX		ΔY		ΔZ	
	cm	ppm	cm	ppm	cm	ppm	cm	ppm
10	62.4	0.51	326.0	7.92	140.8	1.97	76.6	0.84
20	59.4	0.49	304.2	7.39	135.8	1.90	80.8	0.89
30	57.8	0.47	318.8	7.75	169.0	2.36	76.6	0.84
40	58.0	0.47	301.0	7.31	173.4	2.42	82.2	0.90
50	58.8	0.48	287.4	6.98	195.8	2.60	95.4	1.04
60	54.0	0.44	272.2	6.61	197.0	2.75	97.0	1.06
70	53.0	0.43	251.8	6.12	199.8	2.79	95.8	1.05
80	53.6	0.44	244.6	5.94	199.4	2.79	89.0	0.98
90	56.4	0.46	235.6	5.72	187.0	2.61	83.4	0.91
100	58.0	0.47	219.8	5.34	165.8	2.32	76.2	0.84
110	59.2	0.48	199.2	4.84	138.8	1.94	71.8	0.79
120	59.0	0.48	188.8	4.59	127.4	1.78	68.2	0.75
130	59.0	0.48	184.2	4.48	122.6	1.71	65.0	0.71
140	58.8	0.48	188.4	4.58	127.2	1.78	65.4	0.72
150	58.8	0.48	190.4	4.62	128.4	1.79	64.8	0.71
160	57.8	0.47	203.0	4.93	137.0	1.91	63.8	0.70

2. Baseline Components

All the baseline components have repeatabilities better than 10.0 ppm for any observing period except for the Case 1 ΔX, which required 20 minutes of observations (Tables 13, 14, 15, and 16).

It is interesting to note that while the ΔX 2σ values for the first segment of Cases 2, 3, 4, and 5 are less than Case 1's first segment, the final Case 1 2σ value is less than the final segment of any other Case. The final 2σ values for Cases 2, 3, 4, and 5 are greater than the Case 1 2σ values after an equivalent number of observations.

The minimum 2σ levels for ΔX and ΔY occur at or near the end of the observing sessions for Cases 1,2, 4 and 5. For Case 3 the minimum 2σ levels occur after 130 minutes of observations. The minimum ΔZ 2σ level occurs after various observation periods, but generally in the vicinity of 130 to 150 minute observation time, which is between the PDOP minimum and the second PDOP peak. Case 3 behaves in an opposite fashion from the other cases in that its minimum ΔX and ΔY 2σ levels occur at the 150-minute time of observation while its ΔZ minimum occurs at the end of the observation period.

Table 14. ΔX 2-SIGMA VALUES FOR CASES 1, 2, 4, AND 5

Observation Period [min]	Case 1		Case 2		Case 4		Case 5	
	cm	ppm	cm	ppm	cm	ppm	cm	ppm
10	646.4	15.69	347.2	8.45	422.6	10.27	395.2	9.60
20	531.4	12.93	311.4	7.57	343.4	8.34	375.4	9.12
30	345.0	8.41	312.2	7.58	312.2	7.32	375.0	8.87
40	248.2	6.03	311.0	7.31	286.8	6.97	336.2	8.17
50	239.6	5.83	286.0	6.95	251.0	6.10	315.8	7.43
60	230.4	5.59	269.2	6.54	246.8	6.00	272.8	6.63
70	221.2	5.39	246.6	5.99	233.4	5.67	252.8	6.14
80	209.2	5.10	243.2	5.91	212.8	5.17	231.0	5.61
90	195.0	4.74	221.4	5.38	188.4	4.43	224.4	5.45
100	202.0	4.91	194.8	4.73	168.8	4.10	206.6	5.02
110	180.8	4.39	168.8	4.10	159.2	3.87	203.4	4.94
120	162.4	3.94	155.2	3.77	155.6	3.78	-	-
130	141.4	3.44	146.4	3.56	141.4	3.43	-	-
140	134.6	3.26	144.4	3.51	139.8	3.40	-	-
150	129.0	3.11	133.0	3.23	-	-	-	-
160	129.4	3.14	134.4	3.27	-	-	-	-
170	121.8	2.96	-	-	-	-	-	-
175	121.8	2.96	-	-	-	-	-	-

Table 15. ΔY 2-SIGMA VALUES FOR CASES 1, 2, 4, AND 5

Observation Period [min]	Case 1		Case 2		Case 4		Case 5	
	cm	ppm	cm	ppm	cm	ppm	cm	ppm
10	110.8	1.55	204.0	2.85	244.2	3.41	325.0	4.54
20	130.4	1.82	191.2	2.67	224.2	3.13	311.4	4.34
30	140.8	1.97	190.6	2.67	220.4	3.08	298.4	4.17
40	130.8	1.83	193.2	2.70	221.0	3.09	264.8	3.70
50	135.4	1.89	192.2	2.69	212.0	2.96	237.0	3.31
60	142.8	1.99	188.6	2.63	203.8	3.00	200.0	2.79
70	144.4	2.02	185.2	2.59	214.6	2.85	181.4	2.53
80	144.6	2.02	185.0	2.58	181.6	2.54	170.2	2.38
90	145.4	2.03	173.4	2.42	147.4	2.06	177.2	2.48
100	145.0	2.10	152.4	2.13	133.8	1.87	174.6	2.44
110	139.0	1.94	127.6	1.78	124.6	1.74	182.2	2.55
120	126.8	1.77	115.2	1.61	124.8	1.74	-	-
130	108.0	1.51	110.6	1.55	119.0	1.66	-	-
140	102.6	1.43	112.6	1.57	120.4	1.68	-	-
150	100.0	1.40	109.0	1.52	-	-	-	-
160	101.8	1.42	118.0	1.65	-	-	-	-
170	100.0	1.40	-	-	-	-	-	-
175	101.8	1.42	-	-	-	-	-	-

Table 16. ΔZ 2-SIGMA VALUES FOR CASES 1, 2, 4, AND 5

Observation Period [min]	Case 1		Case 2		Case 4		Case 5	
	cm	ppm	cm	ppm	cm	ppm	cm	ppm
10	73.6	0.81	65.2	0.76	92.8	1.02	88.0	0.97
20	78.0	0.86	73.4	0.81	87.4	0.96	74.6	0.82
30	53.8	0.59	69.8	0.77	82.8	0.91	65.2	0.72
40	54.6	0.60	71.6	0.79	78.4	0.86	57.8	0.63
50	55.4	0.61	71.6	0.79	72.0	0.79	49.2	0.53
60	60.2	0.66	68.4	0.75	68.4	0.75	47.8	0.52
70	62.6	0.69	63.8	0.70	65.0	0.71	52.2	0.57
80	61.0	0.67	59.8	0.70	59.8	0.66	53.2	0.58
90	59.2	0.65	58.2	0.64	55.2	0.61	56.2	0.62
100	58.0	0.64	55.4	0.61	53.2	0.58	58.2	0.64
110	56.6	0.62	53.4	0.59	52.2	0.57	59.4	0.65
120	55.8	0.61	52.8	0.58	53.6	0.59	-	-
130	54.4	0.60	52.4	0.58	54.0	0.59	-	-
140	53.8	0.59	54.2	0.59	53.6	0.59	-	-
150	53.6	0.59	54.4	0.60	-	-	-	-
160	56.0	0.61	53.4	0.59	-	-	-	-
170	56.6	0.62	-	-	-	-	-	-
175	56.0	0.61	-	-	-	-	-	-

3. Standard Deviation of the Mean

The repeatability values can be used to estimate the standard deviations of the mean errors given in Tables 7 through 11 by using Equation (5.2). The values of Tables 12 through 16 should be divided by $\sqrt{28}$ (where 28 is the sample population) to compute the standard deviations of the means (at the 2σ level). Generally, the repeatabilities were about five times the magnitudes of the mean errors; therefore, the uncertainties of the mean errors are on the order of the mean errors themselves. Allowing for the 0.1 ppm uncertainty in the baseline and the baseline components and for the possible standard deviation of the means, accuracies to better than 1.0 ppm for the slope distances and 10.0 ppm for the baseline components remain valid.

D. ERROR EFFECTS

1. 7-Day Means

Because of the observations were made over a long period of time, Case 1 was subdivided into four groups comprised of seven consecutive observation days to study trends in the slope distance error to identify the contribution of various error sources to

optimizing observing times. The results for the slope distance error are presented in Table 17.

Table 17. CASE I ERROR: 7-DAY MEANS

Observation Period [min]	Group 1		Group 2		Group 3		Group 4	
	cm	ppm	cm	ppm	cm	ppm	cm	ppm
10	80.5	0.65	-19.0	-0.15	53.5	0.43	29.0	0.24
20	62.6	0.51	21.1	0.17	26.9	0.22	10.9	0.09
30	42.8	0.35	1.4	0.01	26.3	0.21	16.4	0.13
40	30.6	0.25	-8.0	-0.07	27.3	0.22	10.4	0.08
50	24.3	0.20	-12.9	-0.10	22.0	0.18	6.1	0.05
60	21.5	0.17	-18.2	-0.15	16.1	0.13	1.8	0.01
70	17.8	0.14	-24.6	-0.20	10.7	0.09	-0.8	-0.01
80	13.2	0.11	-25.4	-0.21	6.1	0.05	-5.9	-0.05
90	10.2	0.08	-27.6	-0.22	2.6	0.02	-9.2	-0.07
100	10.7	0.09	-30.9	-0.25	0.8	0.01	-12.0	-0.10
110	6.4	0.05	-36.4	-0.30	-2.4	-0.02	-16.2	-0.13
120	2.0	0.02	-40.7	-0.33	-6.1	-0.05	-19.0	-0.15
130	-0.6	-0.00	-43.6	-0.35	-6.6	-0.05	-21.6	-0.18
140	-2.1	-0.02	-43.5	-0.35	-6.3	-0.05	-21.8	-0.18
150	-2.3	-0.02	-42.5	-0.35	-5.6	-0.05	-21.8	-0.18
160	-1.6	-0.01	-40.6	-0.33	-4.8	-0.04	-21.0	-0.17
170	-0.2	-0.00	-38.3	-0.31	-3.4	-0.03	-20.5	-0.17
175	0.7	0.01	-37.4	-0.30	-2.3	-0.02	-20.1	-0.16

The seven-day mean slope distance errors remain below 1.0 ppm for all groups for any observation period. The differences between the groups are mainly in the predominance of negative errors in Groups 2 and 4 while Groups 1 and 4 have predominantly positive errors.

To account for the change in the characters of the groups, the change in the major sources of error are examined.

2. Ephemeris Errors

Examining the AODE (Age of Data Ephemeris) for all satellites during the eight-week observing period, showed that the oldest AODE for a single satellite was nine hours, but most were less than five hours. Averaging the AODE for all satellites for each observing day showed a range of seven hours during the eight weeks of observations (Figure 6). Assuming 12 hours is the largest AODE, the maximum ephemeris linearization error would be 50 cm. Using Equation (2.3) results in 0.025 ppm baseline relative error.

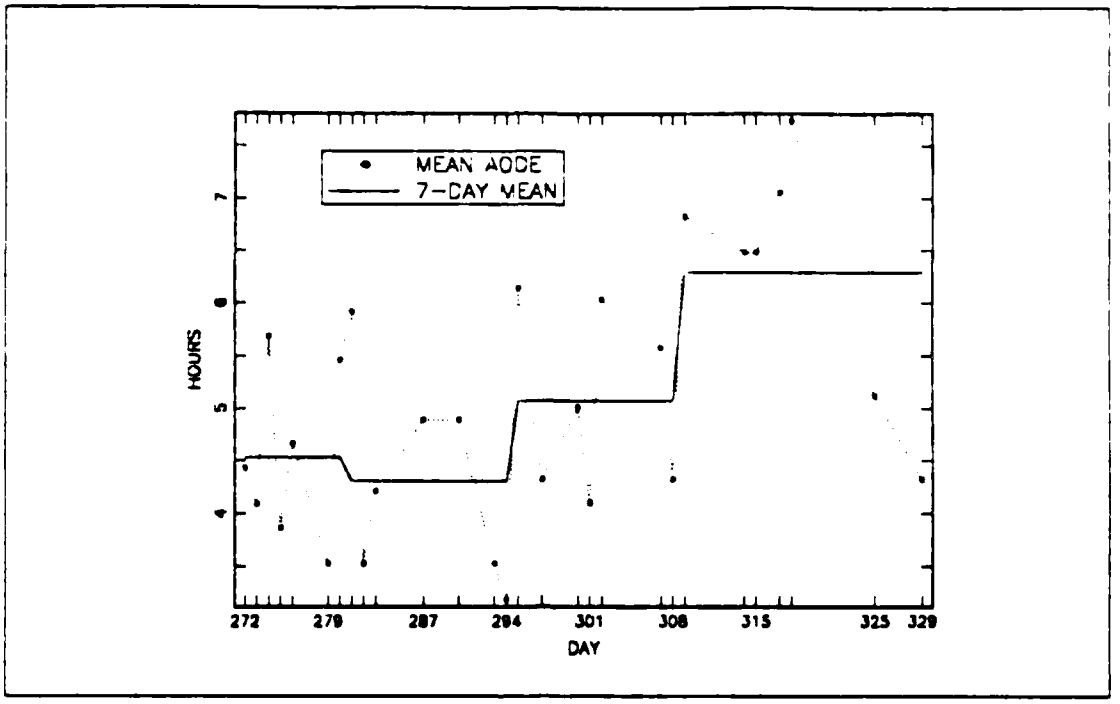

Figure 6. Mean age of data (ephemeris)

The changes in the seven-day mean AODE's do not correspond well to the changes in the groupings, especially as the largest change in AODE from group 3 to 4 does not correspond to a similar change in the group 3 to 4 mean slope distance errors. This is not surprising because while the change is *relatively* large, the magnitude of the orbital errors is expected to be small.

The ephemeris error will appear as a bias during any one observing session. By averaging over eight weeks some of the errors will cancel and appear as variance. Because of the short observing sessions, little variation in the ephemeris error is expected during any single sessions

3. Ionospheric Errors

All the observing sessions completed well before 1600 local standard time and approached the normally ionospheric activity minimum of 0600 (Figure 7). The near north-south orientation of the Monterey-Sand Point baseline places both stations in the same time zone, so that ionospheric errors between the two stations will be correlated to some degree and reduced in the differencing.

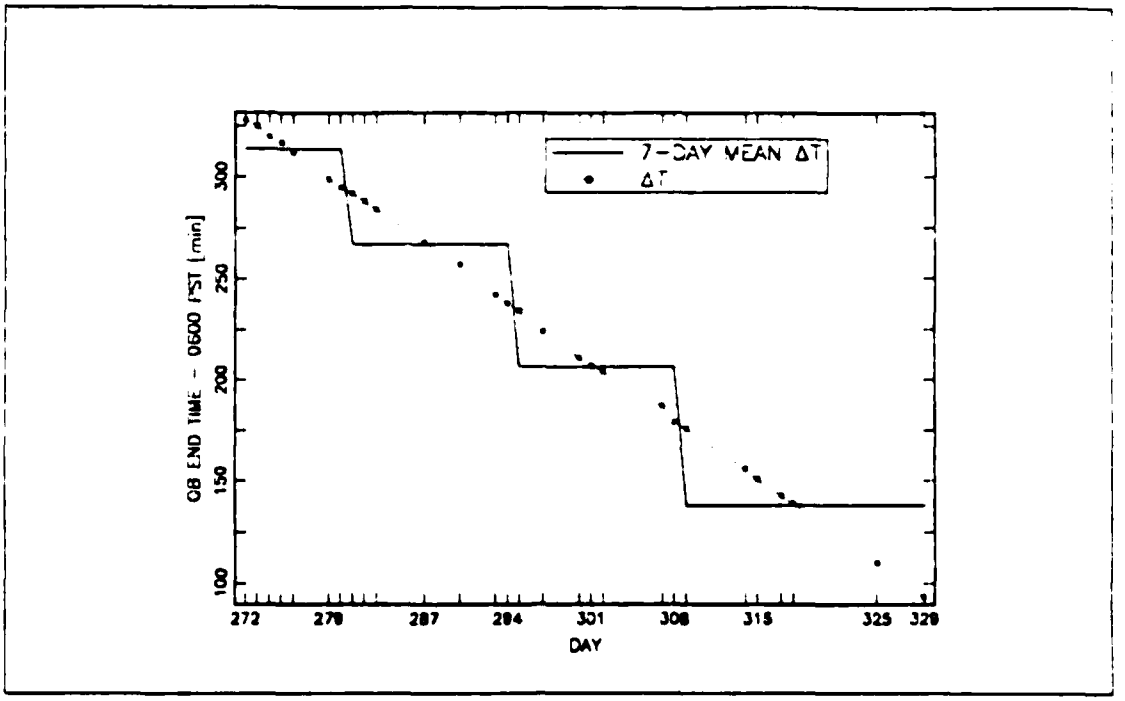

Figure 7. **Difference between observation end time and 0600 PST**

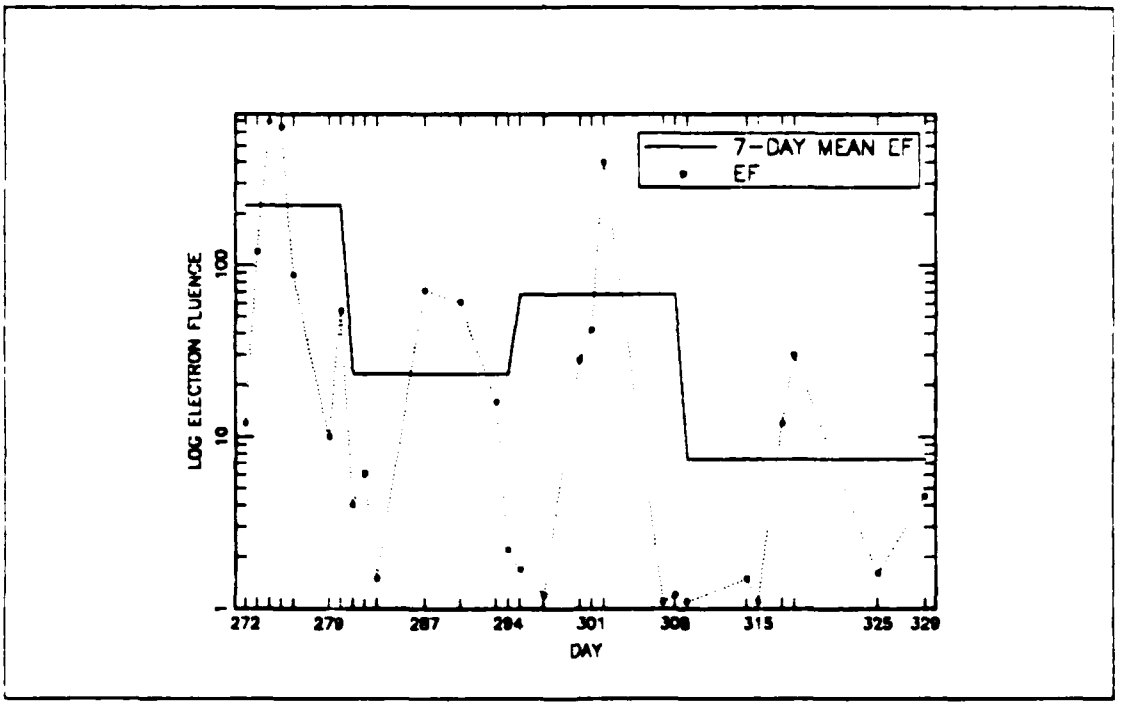

Figure 8. Electron fluence: Units $electrons - cm^{-2} - day^{-1} - sr^{-1}$.

The weekly *Preliminary Report and Forecast of Solar Geophysical Data* [Space Environment Services Center, 1987] for the eight weeks of the observations described the solar and geomagnetic activity as generally quiet or low.

Though the observing period occurred during a general lull in ionospheric activity, there are two ionospheric effects that can be easily examined: the diurnal effect as the observing periods occur closer to the diurnal ionospheric activity minimum and sporadic effects from electron fluxes. The change in ionospheric range error for the eight-week observing period was computed from Henson and Collier [1986, Equation (3)] using the difference in Total Electron Content (TEC) determined from Spilker [1980, Figure 1-11] and Henson and Collier [1986, Figure 2] for the mean observation times for the first and last groups. The maximum change in range error, because of diurnal ionospheric changes from the first to the last week, is approximately 1.5 m which by Equation (2.3) is equivalent to a change in the relative baseline error of only 0.075 ppm.

While the 0.075 ppm trend is not discernible because of the 0.1 ppm uncertainty in the baseline and the larger uncertainties in the measurements, the mean number of observations (Table 5) increased with each later group. The mean number of triple difference observations available were : 1519 ±45, 1522 ±22, 1691 ±124, and 1726 ±174 for the first through the last groups respectively. The increased number of observations could be attributed to stronger signal-to-noise ratio with the reduced ionospheric dispersion as the observations approach the diurnal ionospheric activity minimum.

The group to group changes did not show an apparent trend, but alternated between predominantly negative and positive mean slope distance errors indicating a sporadic effect, or complex interaction between the error sources. To examine sporadic ionospheric effects, daily Electron Fluence (EF) from the weekly *Preliminary Report and Forecast of Solar Geophysical Data* [Space Environmental Services Center, 1987], and seven-day means of the EF were computed (Figure 8). Electron fluence ($electrons - cm^{-2} - day^{-1} - sr^{-1}$) is the daily average of electron flux with energies greater than 2 Mev as measured by the GOES-7 satellite. High values of the seven-day mean EF corresponded to predominantly positive seven-day mean slope distance errors (Groups 1 and 3), and low mean EF corresponded to negative mean slope distance error.

4. Tropospheric Errors

Refractivity, N, was computed using the meteorological parameters from the time closest to the middle of each observation session and Remondi [1984, equations 2.30 and 2.31]. Possible indicators of the influence of the troposphere upon the baseline

solution are the difference in refractivity, ΔN, between the baseline stations (Figure 9) and the mean N of both stations (Figure 10). The difference can indicate the level of correlation of the tropospheric errors. Correlated tropospheric errors are reduced in differencing. The mean N ($\overline{N}$) will indicate the magnitude of the refraction of the carrier signal to both sites.

The changes in the difference in the seven-day mean N (Figure 9) did not have an apparent correspondence to the changes in the seven-day group mean slope distance errors. Instead $\overline{N}$ shows a pattern similar to the group slope distance errors (Figure 10). High mean refractivity corresponded to positive mean slope distance errors (Groups 1 and 3), and low mean refractivity corresponded with negative mean slope distance errors. The difference between the high and the low mean $\overline{N}$ are small and do not readily account for the magnitude of the changes.

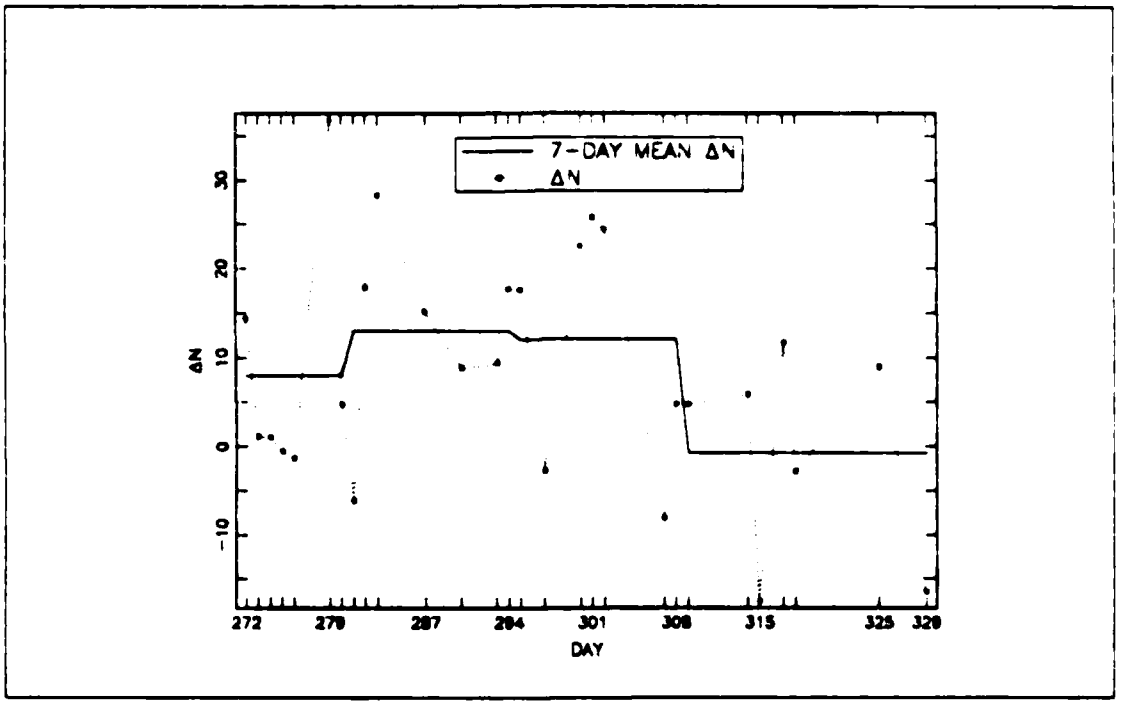

Figure 9. Difference in refractivity between Monterey and Sand Point

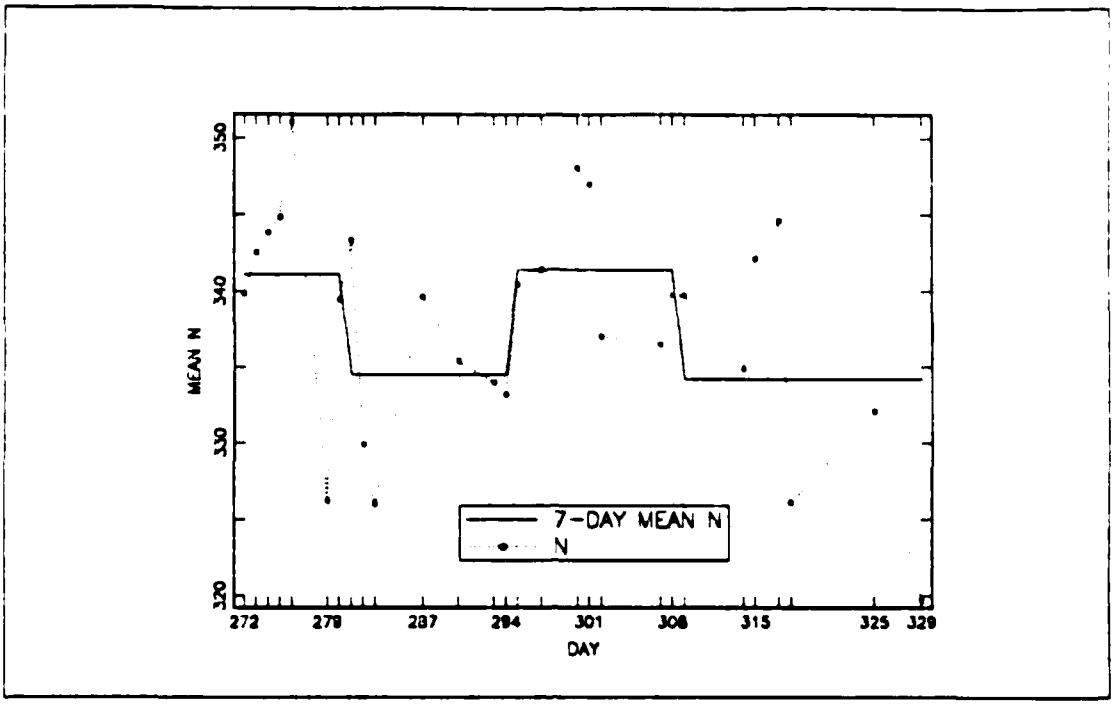

Figure 10. Mean Monterey-Sand Point refractivity

5. 7-Day Repeatability

The Group repeatabilities could not be given a general characterization as the Group means were because the was no consistent pattern to the Group-to-Group changes in their repeatabilities. For completeness, the 2σ values for the various error sources are presented in Table 18, and the Group 2σ values are presented in Table 19.

Table 18. GROUP 2-SIGMA VALUES FOR THE ERROR SOURCES

Error Source	Group 1	Group 2	Group 3	Group 4
AODE [*hours*]	1.6	2.0	1.6	2.4
Observation End Time - 0600 PST [*minutes*]	24.8	45.0	37.6	56.8
Electron Fluence [$electrons - cm^{-2} - day^{-1} - sr^{-1}$]	610.0	59.6	294.8	21.4
ΔN	27.4	21.2	27.8	23.8
$\bar{N}$	15.2	10.6	9.0	17.8

Table 19. CASE 1: 2-SIGMA VALUES, 7-DAY GROUPINGS

Observation Period [min]	Group 1		Group 2		Group 3		Group 4	
	cm	ppm	cm	ppm	cm	ppm	cm	ppm
10	129.8	1.06	81.2	0.66	155.4	1.26	232.0	1.89
20	89.4	0.73	110.2	0.90	141.8	1.15	124.8	1.01
30	61.8	0.50	64.0	0.52	108.2	0.88	89.6	0.73
40	60.8	0.49	56.2	0.46	80.6	0.70	64.8	0.53
50	58.0	0.47	53.6	0.44	72.6	0.59	52.4	0.43
60	59.8	0.49	53.4	0.43	65.4	0.53	45.6	0.37
70	62.0	0.50	46.2	0.38	60.2	0.49	44.8	0.36
80	57.0	0.46	49.0	0.40	53.4	0.43	48.2	0.39
90	57.0	0.46	47.4	0.39	51.4	0.42	47.6	0.39
100	55.6	0.45	46.0	0.37	50.4	0.41	50.0	0.41
110	57.4	0.47	46.8	0.38	50.4	0.41	53.2	0.43
120	61.8	0.50	46.8	0.38	48.2	0.39	55.4	0.45
130	64.6	0.53	44.4	0.36	45.4	0.37	58.0	0.47
140	65.0	0.53	43.0	0.35	43.4	0.35	60.2	0.49
150	64.4	0.53	43.4	0.35	42.2	0.34	60.2	0.49
160	63.4	0.52	42.8	0.35	42.6	0.35	59.2	0.48
170	62.8	0.51	42.6	0.35	43.8	0.36	58.6	0.48
175	63.0	0.51	41.6	0.34	45.0	0.37	57.6	0.47

E. EFFECTS OF THE C/A CODE

The best C/A code position for Monterey was extracted from each observing session for comparison with the carrier phase results. The coordinates of Sand Point were subtracted from the 28-day mean of the Monterey C/A code coordinates to form the baseline components. The slope distances were computed from the square root of the sum of the squares of the baseline components. The mean errors of the C/A code derived baseline were on the order of the carrier phase mean errors, but the 2σ levels are several times greater than the carrier phase results (Table 20). These results are for one instantaneous position determination and would improve with time averaging within the observing period or Doppler-smoothing.

The C/A code has its most significant impact upon the differenced carrier phase solutions when there are few carrier phase observations. Table 21 shows that reprocessing the carrier phase observations was required for several segments because either more than ten percent of the observations were rejected or the slope distance solution sigma was greater than 10 m, and that all the reprocessed segments were confined to the first two segments.

Table 20. BEST C/A CODE RESULTS AND ERRORS

Component	Distance (m)	Relative Error (ppm)
ΔX	-411587.334	-8.2 ±30.0
ΔY	-715776.997	0.8 ±28.5
ΔZ	-911739.358	-3.3 ±17.7
Slope Distance	1230044.511	-0.6 ± 7.2

Table 21. CASE 1: DATA SEGMENTS BEFORE AND AFTER REPROCESSING

Day	Segment	Total Obs	Before		After		
			Rejected Obs	Slope Distance (m)	Rejected Obs	Slope Distance (m)	Edit Multiplier
Case 1							
272	1	62	14	1230050.192	0	1230045.846	99
275	1	42	17	1230268.988	0	1230045.294	5
276	1	51	5	1230047.276	0	1230047.020	99
280	1	61	41	1230227.492	0	1230045.717	99
280	2	110	44	1230093.548	0	1230045.915	5
287	1	48	6	1230048.636	0	1230045.326	99
294	2	124	23	1230044.230	12	1230046.146	5
308	1	45	* 2	1230042.920	0	1230045.972	99
Case 2							
314	1	78	56	1230074.209	0	1230045.282	3.5
Case 3							
314	1	59	37	1230074.209	0	1230045.373	3.5
Case 4							
281	1	78	22	1230034.198	0	1230045.082	3.5
281	2	169	47	1230041.504	11	1230045.031	3.5
282	1	62	20	1230039.213	0	1230045.024	3.5
Case 5							
287	2	159	43	1230043.418	3	1230045.177	3.5
308	1	86	24	1230043.047	0	1230045.472	3.5
314	1	52	* 1	1230051.620	0	1230048.000	99.0

The carrier phase solutions were improved by the least-squares processing of the pseudoranges to obtain better initial antenna position estimates and also to correct the

carrier phase time-tags. All the Case 1 reprocessed segments were improved by forcing the processing program to accept more carrier phase observations by increasing the edit multiplier.

Because of the success of improving the solutions by the pseudorange pre-processing, all segments for three days (276, 287, and 294) were reprocessed to see if their already acceptable solutions would improve. The solutions either did not change or became slightly less accurate.

F. COMPARISON WITH PREVIOUS STUDIES

Remondi [1984] concluded that 100 ppm accuracy was achievable in 30 minutes and 10 ppm, in one hour - regardless of baseline length - based upon single-frequency, single difference solutions using precise ephemerides over baselines less than 100 km. To study the required observation times for various accuracies, he partitioned his data into 15-minute observation spans. While decorrelated triple differences would be capable of performing relative geodesy at 1 ppm level, correlated triple differences may provide 5-10 ppm or better [Remondi, 1985].

Some long baseline surveys include:

Bock *et al.* [1984] achieved 2 ppm accuracy in closure of a transcontinental net aided by external atomic clocks using 10 hours of single frequency, single difference observations.

Cannon *et al.* [1985] achieved 0.1 to 0.7 ppm repeatability using single frequency non-differenced network solutions without ionospheric correction for 1700-km baselines between two California stations and Calgary, Alberta, Canada over a four-day period. The range in repeatability was attributed to satellite clock errors. They also found that the largest errors occurred in the ΔX component.

Mader and Abell [1985] found that single frequency long baseline GPS results using single differenced carrier phase observables agreed to one ppm with VLBI measured baseline lengths. Their 2-day repeatability was 0.24 ppm.

Goad *et al* [1985] measured a 1302-km baseline between California and Texas to better than 1.0 ppm compared to the VLBI measured distance, and their two-day repeatability was better than 0.5 ppm.

Bertiger and Lichten [1987] achieved 6 parts per **billion** repeatability over a 1314-km east-west baseline over separate four and seven-day periods using dual-frequency receivers with a fiducial network for orbit determination, and some water vapor radiometers.

Except for the Bertiger and Lichten [1987] results, the Case 1 results are competitive with the above studies despite the inherent low resolution and the added burden of the correlations of the correlated triple differences. A possibility for the optimum results of Case 1 is that a good solution is insured by setting both receivers to their known WGS84

coordinates. For real-time surveys, one end of the baseline will usually not be known to one meter accuracy.

During the eight-week observation period, the third 4000SX was delivered to NPS. The antenna was installed on the same rooftop, but approximately 35 m to the north of the Monterey antenna. Two days of data using Monterey as the reference station were used to fix the location of the new antenna. On Day 294, the new receiver's coordinates were offset 37 m, equivalent to 30 ppm baseline error. The difference between the offset antenna and Monterey solutions for the baseline to Sand Point is 0.7 ppm for the first segment (Figure 11).

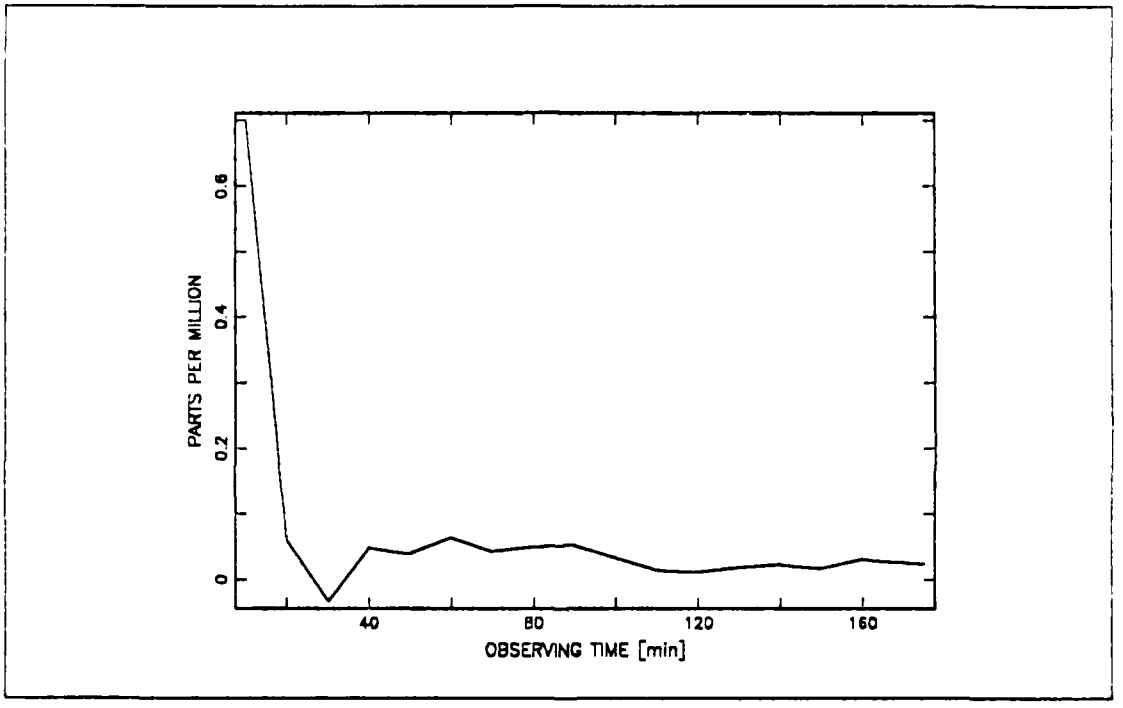

Figure 11. Results of station 2 offset

For the remaining segments the difference is about 0.05 ppm. The first segment will be more affected by receiver offset because the small number of carrier phase observations will be sensitive to the initial position estimate provided by the C A code. The C A code, in turn, will be sensitive to the receiver coordinates because the receiver will compute the slant range to the satellites using those coordinates.

G. MISSING EPOCHS

Missing epochs prevented a sixth case study in which the number of observations are reduced by flagging the data. The sixth case study was to have studied the effects

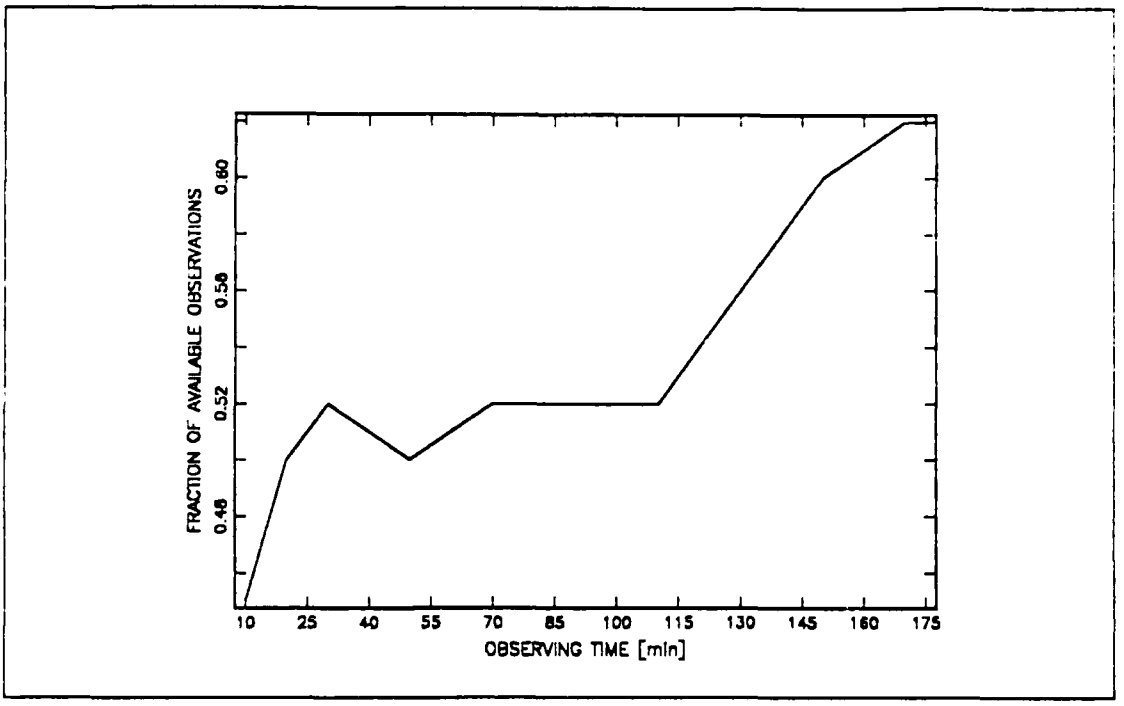

Figure 12. Fraction of available triple difference observations

of reducing the number of observations without changing the geometry. Several days of data were processed in which only every other epoch was to be used in the processing. An hour of data was needed to obtain enough triple difference observations to consistently have less than 10% of the triple difference observations rejected and slope distance σ's less than 10 m. This inability to form a reliable solution indicated a lack of carrier phase observations, so the number of observations were counted.

The mean number of observations (accumulative) available for each segment, as a fraction of the maximum number of triple difference observations remained steady until 120 minutes when it increased (Figure 12). The maximum number of triple difference observations is: $M_{TD} = (n_t - 1)(n_s - 1)$ where:

M_{TD} maximum number of triple difference observations

n_t number of observations epochs

n_s number of observed satellites

Solutions using only 10 minutes of data at a time were examined to investigate the rise in available observations after 120 minutes. A curious phenomenon was discovered that while SV 6 was being tracked at Sand Point between five and ten of every 40 epochs

were lost (Figure 13). As soon as SV 6 was no longer being tracked at Sand Point, no complete loss of epochs was observed (Figure 14).

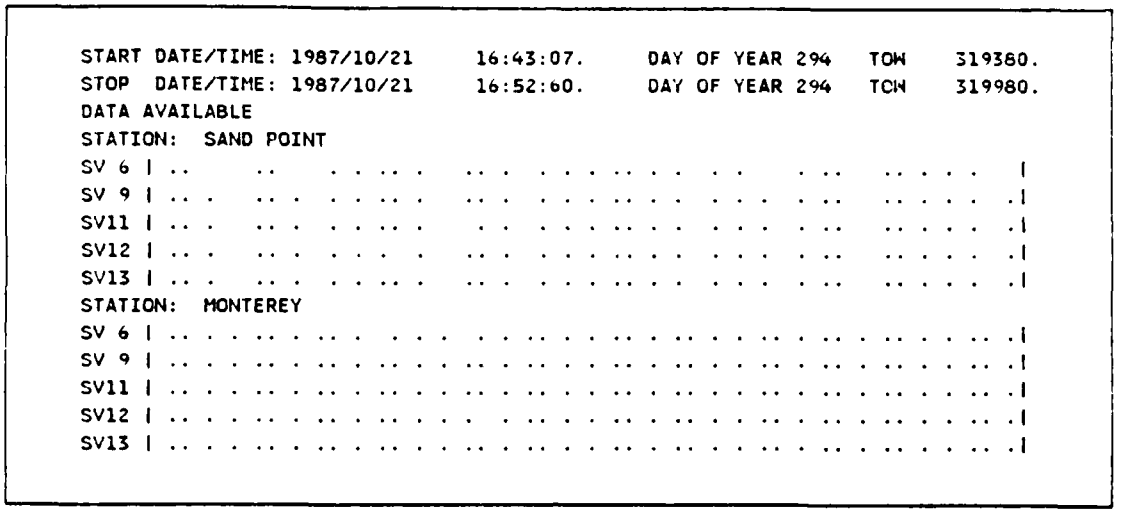

Figure 13. Missing epochs while tracking SV 6: Each dot represents one observation; each column, one epoch. Sand Point is missing epochs 4, 8, 14, ., 26, 30, 34, and 40. From *Trim640 output.*

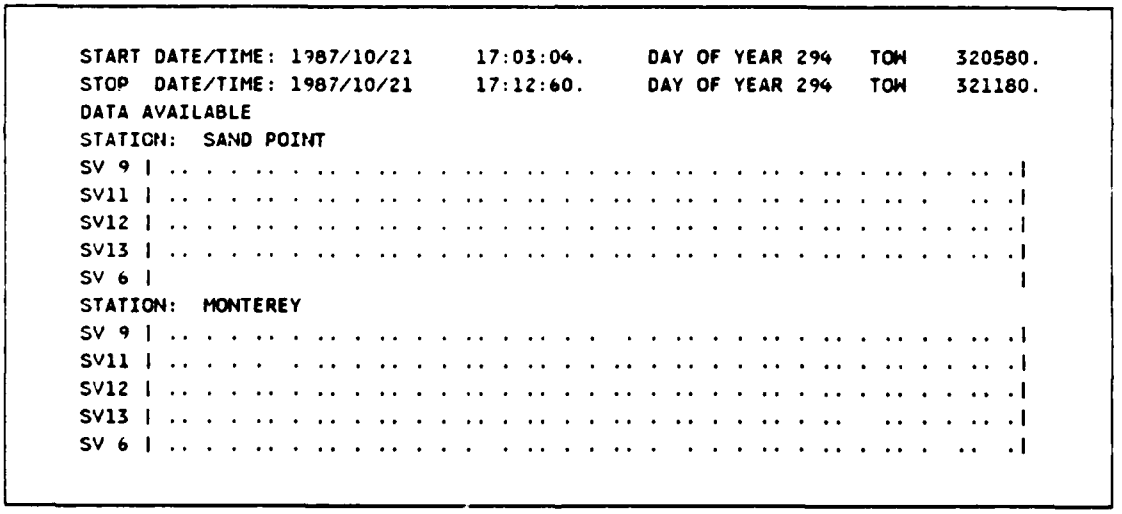

Figure 14. Continuous tracking without SV 6.: No missing epochs at Sand Point.

The phenomenon is not multipath interference because it affects all satellite at each epoch. A simultaneous outage would suggest interference from some other emitter at or near 1540 MHz, if the outages continued throughout the observation session rather than being limited to when SV 6 was being tracked. No physical cause for the outages

is readily available, and the data have been forwarded to Trimble Navigation Ltd for further evaluation.

H. DILUTION OF PRECISION AND RANGE ERRORS

The case studies showed that the accuracy and precision of the slope distance were improved by using observations associated with the infinite PDOP peak rather than either the PDOP minimum or the secondary PDOP rise near the end of the observing sessions, and that improvements in the slope distance accuracy could be achieved using fewer observations when observations are made through the infinite PDOP peak. Precision and accuracy of the solutions are dependent on geometry (fixed with respect to Case 1 time) and error sources rather than the number of observations (fixed with respect to length of observing period).

The mean slope distance errors were governed by the ionospheric and tropospheric errors opposing each other. Early and late observations had positive mean errors while the errors about the infinite PDOP peak were negative. Tropospheric errors are partially corrected by the modified Hopfield model while the ionospheric errors remain uncorrected, and as the satellites reach the infinite PDOP peak the full impact of the ionospheric errors project upon the baseline.

The rôle reversal of the PDOP peak from point positioning to relative positioning requires some investigation. Because PDOP reflects the strength of the satellite geometry for a single station, the investigation should begin with the satellite-baseline (two station) geometry by examining a simple projection of errors upon a baseline using a single satellite whose track is directly over the baseline (Figure 15).

From the law of cosines:

$$b_T^2 = \rho_1^2 + \rho_2^2 - 2\rho_1\rho_2 \cos\gamma \tag{6.1}$$

where:

- b_T true baseline
- ρ_1 range from station 1 to the satellite
- ρ_2 range from station 2 to the satellite
- γ angle between ρ_1 and ρ_2

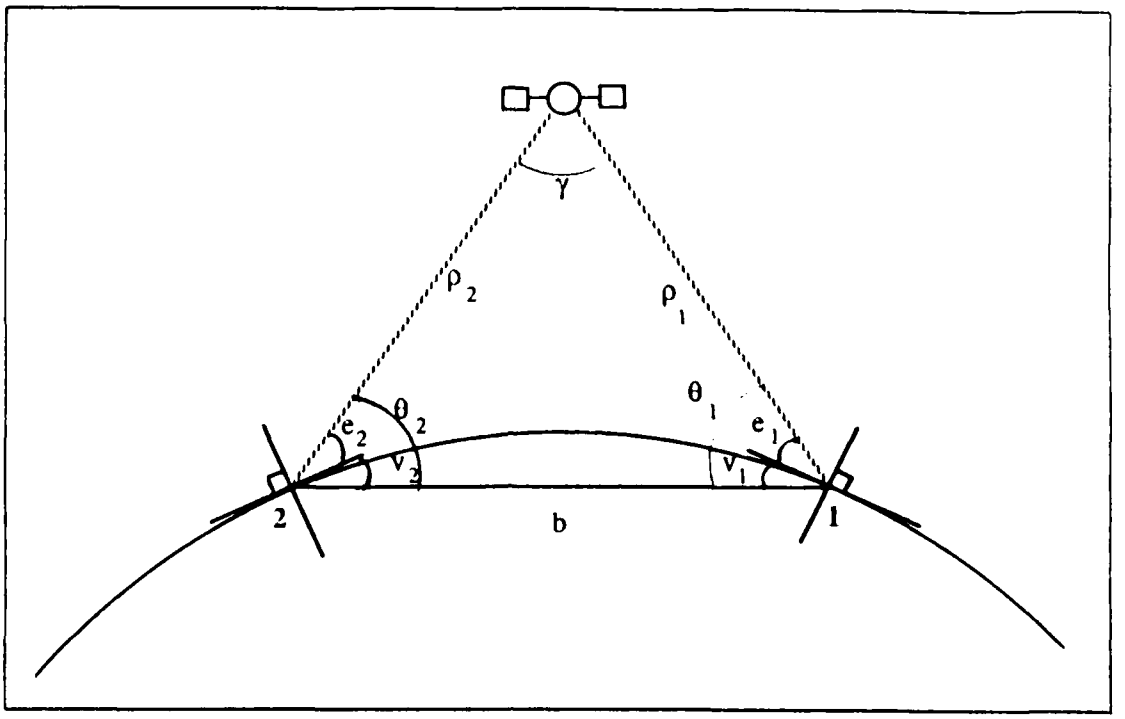

Figure 15. Relative positioning geometry: Not drawn to scale.

Similarly we define a measured baseline, b_M:

$$b_M^2 = (\rho_1 + E_{\rho 1})^2 + (\rho_2 + E_{\rho 2})^2 - 2(\rho_1 + E_{\rho 1})(\rho_2 + E_{\rho 2}) \cos \gamma \tag{6.2}$$

where:

$E_{\rho 1}$ error in ρ_1

$E_{\rho 2}$ error in ρ_1

Subtracting the square root of (6.1) from the square root of (6.2), and letting $\cos \gamma = 1$, gives:

$$\frac{b_M - b_T}{b_T} = \sqrt{1 + \frac{\Delta E_\rho^2}{b_T^2} + 2\frac{\Delta \rho \Delta E_\rho}{b_T^2}} - 1 \tag{6.3}$$

where $\Delta E_\rho = E_{\rho 2} - E_{\rho 1}$ and $\Delta \rho = \rho_2 - \rho_1$. From (6.3), $\Delta \rho$ acts as an amplification factor for the difference in the range errors (ΔE_ρ). As a satellite approaches the mid-point of a baseline, $\Delta \rho \rightarrow 0$ and $b_T >> \Delta E_\rho$.

Similar arguments can be extended to point positioning using two satellites at one epoch or two epochs of one satellite by inverting the geometry of Figure 15, but the reduction in range errors would apply to point positioning as well.

The effects of γ have been ignored because γ is small. From the law of sines:

$$\sin \gamma = \frac{b \sin \theta}{\rho} \tag{6.4}$$

where $\theta = e + v$. e is the elevation angle to the satellite and v is the vertical angle between the slope distance and the local horizon. Expanding $\sin\theta$ as $\sin e \cos v + \cos e \sin v$, and $(\sin e \cos v) >> (\cos e \sin v)$ because $\cos v \cong 1$ (v is -5° for the 1230 km baseline), then $\sin\theta$ can be approximated by $\sin e$. Approximating b by 1230 km and ρ by 20000 km, then, by the law of sines, γ is approximately 1° when e is 15°; by the law of cosines, γ is approximately 2.5° when the satellite is at the baseline midpoint.

With $\cos 1° \cong 0.9998$ and $\cos 2.5° \cong 0.9991$, a very insignificant change, most of the deviation of the measured baseline from the true baseline must come from the error difference factor, ΔE_ρ. Most importantly having satellites at high elevation angles with respect to the termini of the baseline is ***not*** detrimental to relative positioning as high elevation angles are for point positioning.

A second area of investigation is the path dependent errors. The ionospheric and tropospheric errors, approximated by cosecant functions of the elevation angle, are minimized at high elevation angles. Simultaneous high elevation angles for both stations is another by-product of high PDOP.

Finally, the effects of differencing must be explored. Qualitatively, when the satellites are bunched close together at high PDOP (Figure 3), some of the correlation in errors that was lost in lengthening the baseline is restored. The change in tropospheric and ionospheric errors with time will also be minimized because:

$$\frac{d \csc e}{dt} = \frac{-\cos e}{\sin^2 e} \frac{de}{dt} \tag{6.5}$$

and high elevation angles minimize Equation (6.5). Such time derivative minimization of errors, will greatly affect the triple difference because the triple difference is itself a time difference.

The sum of the elevation angles for all satellites at both stations (Table 22) reaches a maximum after 70 minutes of observations, which is ten minutes later than the PDOP

peak. The minimum variance is achieved in the 80 to 90 minute Case 1 time. The running mean of the sum of the elevation angle peaks at the 100 minute observing time while the running mean elevation angle reaches a local maximum in the 80 to 100 minute range. The running means provide a better estimator of the behavior of the accuracy and precision because of the accumulation of observations.

Table 22. ELEVATION ANGLES

Observation Time	Number of SV's	Sum of Elevation Angles	Mean Elevation Angle	Running Mean of Sum	Running Mean Elevation Angle
0	8	404	50.5	404	50.5
10	8	446	55.8	425	53.1
20	10	509	50.9	453	52.3
30	10	525	52.5	471	52.3
40	10	547	54.7	486	52.8
50	10	559	55.9	498	53.4
60	10	569	56.9	508	53.9
70	10	562	56.2	515	54.2
80	10	557	55.7	520	54.4
90	10	548	54.8	523	54.4
100	10	535	53.5	524	54.3
110	10	517	51.7	523	54.1
120	8	505	50.5	519	54.7
130	8	464	58.0	516	54.9
140	8	452	56.5	511	55.0
150	8	441	55.1	507	55.1
160	8	418	52.3	502	55.0
170	8	396	59.4	496	54.8

V. CONCLUSIONS AND RECOMMENDATIONS

A. CONCLUSIONS

Following a recommendation by Remondi [1984] that more testing of the accuracies of triple difference carrier phase measurements was needed, I studied the optimized GPS observation times required to achieve geodetic accuracies by partitioning observation periods for a 1230-km baseline into ten-minute segments and changing the length and starting time of observations. Accuracy was determined by comparing measured baseline values with reference values obtained by locating the ends of the baselines from very precise VLBI horizontal control points using double difference GPS carrier phase measurements over short baselines.

The 1230-km baseline was directly measured for 28 days over a period of eight weeks using Trimble 4000SX receivers. The Trimble supplied *Trimvec* software was used to process the carrier phase measurements. Using broadcast ephemerides in a fixed orbit, triple difference carrier phase solution with no ionospheric corrections and a tropospheric delay model that used only surface meteorological data, 1.0 part per million (ppm) accuracy in the slope distance was achieved for any observing period with a day-to-day repeatability better than 1.0 ppm (2σ). The ΔX, ΔY, and ΔZ (the components of the baseline parallel to the WGS84 axes) achieved accuracies better than 10.0 ppm for any observing period. ΔY and ΔZ repeatabilities were better than 10.0 ppm for any observing period, while ΔX required 30 minutes of observations to reach 10.0 ppm.

I had not expected to achieve 1.0 ppm accuracy in the slope distance measurements because Remondi [1984] had suggested that 1.0 ppm required dual frequency measurements using highly accurate orbit information and water vapor measurements, and my solutions are further burdened by the correlations of the triple differences. The 1.0 ppm accuracies were on the order of the uncorrelated single frequency results of previous long baseline GPS surveys: Cannon *et al.* [1985], Bock *et al.* [1984], Goad *et al.* [1985], and Mader and Abell [1985].

The unexpected 1.0 ppm accuracy can be attributed to low ionospheric activity because of the orientation of the baseline, the time of year, and the minimum in the sunspot cycle and solar activity during the observing period. Ephemerides errors are considered low because of the low age of the ephemerides. Those ameliorating factors must be considered before applying the results of these case studies to planning surveys

on different baselines at different times of day and year. Ionospheric errors were on the order of the tropospheric errors. The superposition of the opposing ionospheric (shortening) and tropospheric (lengthening) errors reduced mean slope distance errors.

Slope distance errors and observation periods were reduced when GPS observations started near the infinite, symmetric PDOP peak. The reduction of errors about the PDOP peak can be attributed to the simultaneous minimization of range errors, the projection of range errors onto a baseline, satellite and epoch separation. A high sum of the satellite elevation angles for a single station can also be used to determine favorable observing times, as simultaneous high elevation angles correspond to high PDOP values.

My results reconfirm Trimble Navigation's [1987b] recommendation to include the infinite PDOP peak in the observing session; however, I could not confirm the Federal Geodetic Control Committee's [1986] proposal to stop at a GDOP of 5.0. I could not identify any consistent observing stop point that improved accuracy other than to stop when four satellites were no longer available.

When less than 30 minutes of data are used, the goodness of the C/A code has a great effect upon the carrier phase solution because C/A code positions are used to estimate the carrier phase solution and to compute the time tags of the carrier phase measurements. The number of rejected triple difference measurements provided the best indicator of the quality of the C/A code estimates and the carrier phase solutions. Incidences of poor accuracy of the carrier phase solution were found to be caused by poor C/A code estimates. The carrier phase solutions could then be improved by correcting the C/A code solutions, and in turn the carrier phase time tags, by pre-processing the C/A code measurements or accepting more carrier phase measurements. Pre-processing the C/A code measurements did not improve the accuracy of the carrier phase solutions when the number of rejected triple differences was less than 10% or when the solution standard deviation of the slope distance was less than 10 m.

The long-term average of the best pseudorange solutions produced results comparable to the mean carrier phase solution, except that the pseudorange solutions had variances several times the magnitude of the carrier phase solutions.

B. RECOMMENDATIONS

The results of these case studies should be tested on surveys conducted with baselines of varying orientation and length and with different satellite configurations.

Currently, *TRIMVEC* does not support the use of precise ephemerides or the computation of uncorrelated triple differences. Should those capabilities be implemented in the future, or provided by third-party software, the data should be reprocessed and analyzed to isolate the tropospheric and ionospheric error contributions and to improve the baseline component results. Both of those capabilities would allow better insight into the effects of geometry and the tropospheric and ionospheric errors.

The usual rôle of the correlated triple difference is to aid in fixing cycle slips when the receiver loses lock and to provide the initial estimates for the double difference least-squares processing. The current data should be reprocessed in the double difference mode to determine whether the correlated triple difference solution provides sufficient accuracy to fix the cycle slips and estimate the initial integer ambiguities in long baseline surveys.

The standard values used to estimate accuracy could be improved by a more rigorous fixing of the antenna locations. Both sites should be subjected to a network adjustment, either locally or simultaneously (possibly in conjunction with the NGS VLBI crustal motion studies). The extra baselines required for a network solution could be measured using the third Naval Postgraduate School receiver.

Studies should be conducted to determine the effects of using meteorological observations far removed from the Sand Point antenna site. A temporary meteorological station could be set up near the antenna site (possibly in cooperation with the Weather Service Forecast Office (WSFO) located on the grounds of the Western Regional Center or with the nearby University of Washington). Future Naval Postgraduate School GPS surveys would be aided by portable meteorological instruments, preferably that made digital records of the temperature, humidity, and pressure.

Because of the importance of elevation angles to accurate results, studies should be conducted to determine the performance of the *TRIMVEC* supplied tropospheric models(modified Hopfield and Marini) at various elevation angles.

While this study has shown the utility of the *single-station* PDOP, a more complete DOP may provide a better satellite selection aid. Such a complete DOP (or Dilution Of Relative Position (DORP)) should incorporate covariances for baseline components, satellite orbital errors, receiver timing errors, ionospheric and tropospheric delays, uncertainties in the reference station coordinates, and cross-covariances. The DORP would also be formulated with respect to the type of differencing to be used.

Lastly, the amount of data processed for these case studies was limited by the speed of the microcomputer and the necessity of transferring the results to the Naval Postgraduate School mainframe for analysis. As more GPS surveys will be conducted in the future, the demands for processing power will increase. It will become imperative that the processing software be ported to the mainframe or to a networked mini-computer. Those computers will allow multiple access to the software as well as speeding the processing. As an interim measure, the RAM of the current ensemble of microcomputers should be increased to several megabytes. This increase in RAM will allow the use of RAM-disks which will speed up the data loading - which is the most time consuming of the processing procedures.

APPENDIX. BATBLD.BAS LISTING

```
10 REM PROGRAM BATBLD.BAS BY R. BOUCHARD NOV87
20 REM PROGRAM BATBLD:  BUILDS THE BATCH FILE FOR TRIMVEC PROCESSING.
30 REM READS WX OBS FROM SEA.MET FILE
40 REM DAY 283 REQUIRES ITS OWN BATBLD PROGRAM.
50 INPUT "batch file name";OFL$
60 SP$=" "
70 S1$="command /c tbf nodd.tem "
80 OPEN  OFL$ FOR APPEND AS #2
90 DIM A$(18),JD$(29),MM$(29),DD$(29),PH(29),PM(29)
95 REM initialize Julian Day array
100 JD$(1)="272": JD$(2)="273": JD$(3)="274": JD$(4)="275"
: JD$(5)="276"
110 JD$(6)="279": JD$(7)="280": JD$(8)="281": JD$(9)="282"
: JD$(10)="287"
120 JD$(11)="290": JD$(12)="293": JD$(13)="294": JD$(14)="295"
: JD$(15)="297"
130 JD$(16)="300": JD$(17)="301": JD$(18)="302": JD$(19)="307"
140 JD$(20)="308": JD$(21)="309": JD$(22)="314"
145 JD$(23)="315": JD$(24)="317": JD$(25)="318"
147 JD$(26)="325": JD$(27)="329" : JD$(28)="321"
150 MM$(1)="09": MM$(2)="09"
160 FOR I=3 TO 18: MM$(I)="10": NEXT I
170 FOR I=19 TO 28: MM$(I)="11": NEXT I
180 DD$(1)="29": DD$(2)="30": DD$(3)="01": DD$(4)="02": DD$(5)="03"
: DD$(6)="06": DD$(
7)="07": DD$(8)="08": DD$(9)="09": DD$(10)="14": DD$(11)="17"
: DD$(12)="20"
190 DD$(13)="21": DD$(14)="22": DD$(15)="24": DD$(16)="27": DD$(17)="28"
200 DD$(18)="29": DD$(19)="03": DD$(20)="04": DD$(21)="05": DD$(22)="10"
205 DD$(23)="11": DD$(24)="13": DD$(25)="14"
207 DD$(26)="21": DD$(27)="25": DD$(28)="17"
210 A$(1)="a01": A$(2)="a02": A$(3)="a03": A$(4)="a04": A$(5)="a05"
: A$(6)="a06"
220 A$(7)="a07": A$(8)="a08": A$(9)="a09": A$(10)="a10": A$(11)="a11"
: A$(12)="a12"
230 A$(13)="a13": A$(14)="a14": A$(15)="a15": A$(16)="a16"
: A$(17)="a17": A$(18)="a18"
240 FOR I=1 TO 7: PH(I)=19: NEXT I
250 FOR I=8 TO 13: PH(I)=18: NEXT I
260 FOR I=14 TO 21: PH(I)=17: NEXT I
270 FOR I=22 TO 25: PH(I)=16: NEXT I
275 FOR I=26 TO 28: PH(I)=15: NEXT I
280 PM(1)=34: PM(2)=31: PM(3)=26: PM(4)=23: PM(5)=18: PM(6)=5: PM(7)=1
290 PM(8)=58: PM(9)=54: PM(10)=33: PM(11)=22: PM(12)=8: PM(13)=3
: PM(14)=59
300 PM(15)=51: PM(16)=39: PM(17)=35: PM(18)=31: PM(19)=14
310 PM(20)=6: PM(21)=2: PM(22)=42
315 PM(23)=37: PM(24)=29: PM(25)=24: PM(26)=56: PM(27)=39: PM(28)=8
317 REM begin building the batch file for each day.
320 FOR IK=1 TO 28
330 OPEN "i",1,"sea.met"
```

```
340 INF$="sa"+JD$(IK)+" ma"+JD$(IK)
350 S2$=S1$+INF$
360 PRINT "FOR JD:   ";JD$(IK)
370 INPUT "start hour";SH
380 INPUT "start minute";SM
390 PRINT JD$,PH(IK),PM(IK)
400 SH$=STR$(SH)
410 SM$=STR$(SM)
420 PC=SM/60
430 I=1
435 REM Find the WX OB
440 INPUT#1,ID$,IH$,P1(I),T1(I),R1(I),P2(I),T2(I),R2(I)
450 IF((ID$=JD$(IK))AND(SH=VAL(IH$))) THEN 470
460 GOTO 440
470 P1(I)=P1(I)-2 :  T2(I)=(T2(I)-32)*5/9
480 I=I+1
490 INPUT#1,ID$,IH$,P1(I),T1(I),R1(I),P2(I),T2(I),R2(I)
500 IF(ID$<>JD$(IK)) THEN 540
505 REM Subtract 2 mb from SEA ob
510 P1(I)=P1(I)-2!
515 REM Convert NPS Temp to Celsius
520 T2(I)=(T2(I)-32)*5/9
530 GOTO 480
540 IE=I-1
550 REM interpolate WX OBS TO GPS START TIME
560 PR1(1)= P1(1)+(P1(2)-P1(1))*PC
570 PR2(1)=P2(1)+(P2(2)-P2(1))*PC
580 TR1(1)=T1(1)+(T1(2)-T1(1))*PC
590 TR2(1)=T2(1)+(T1(2)-T1(1))*PC
600 RR1(1)=R1(1)+(R1(2)-R1(1))*PC
610 RR2(1)=R2(1)+(R2(2)-R2(1))*PC
615 REM Compute running mean of first hour
620 PR1(2)= (PR1(1)+P1(2))/2
630 PR2(2)=(PR2(1)+P2(2))/2
640 TR1(2)=(TR1(1)+T1(2))/2
650 TR2(2)=(TR2(1)+T2(2))/2
660 RR1(2)=(RR1(1)+R1(2))/2
670 RR2(2)=(RR2(1)+R2(2))/2
680 WT=1-PC
685 REM Compute remaining running means
690 FOR I= 3 TO IE
700 IA=I-1
710 IWT=1+WT
720 PR1(I)=(PR1(IA)*WT + ((P1(IA)+P1(I))/2))/(IWT)
730 PR2(I)=(PR2(IA)*WT + ((P2(IA)+P2(I))/2))/(IWT)
740 TR1(I)=(TR1(IA)*WT + ((T1(IA)+T1(I))/2))/(IWT)
750 TR2(I)=(TR2(IA)*WT + ((T1(IA)+T2(I))/2))/(IWT)
760 RR1(I)=(RR1(IA)*WT + ((R1(IA)+R1(I))/2))/(IWT)
770 RR2(I)=(RR2(IA)*WT + ((R2(IA)+R2(I))/2))/(IWT)
780 WT=IWT
790 NEXT I
800 M1=SM
810 H=SH
820 C=0
830 I=2
840 DHR=PH(IK)-SH: DMIN=PM(IK)-SM
```

```
850 IF(DMIN<0) THEN DHR=DHR-1: DMIN=DMIN+60
860 NP=DHR*6+(DMIN/10)
865 REM Interpolate hourly running means to 10 minute intervals
870 FOR IL=1 TO NP
880 M1=M1+10
890 IF(M1>60) THEN M1=M1-60: H=H+1: I=I+1
900 WT=M1/60
910 IF(M1=60) THEN M1=M1-60: H=H+1: I=I+1
920 MP=M1
930 HP=H
940 IWT=1-WT
950 IA=I-1
960 PW1=PR1(IA)*(IWT)+PR1(I)*WT
970 PW1=INT((10*PW1)+.5)/10
980 PW2=PR2(IA)*(IWT)+PR2(I)*WT
990 PW2=INT((10*PW2)+.5)/10
1000 TW1=TR1(IA)*(IWT)+TR1(I)*WT
1010 TW1=INT((10*TW1)+.5)/10
1020 TW2=TR2(IA)*(IWT)+TR2(I)*WT
1030 TW2=INT((10*TW2)+.5)/10
1040 RW1=RR1(IA)*(IWT)+RR1(I)*WT
1050 RW1=INT((10*RW1)+.5)/10
1060 RW2=RR2(IA)*(IWT)+RR2(I)*WT
1070 RW2=INT((10*RW2)+.5)/10
1080 REM convert to strings
1090 PS1$=LEFT$(STR$(PW1),7)
1100 PS2$=LEFT$(STR$(PW2),7)
1110 TS1$=LEFT$(STR$(TW1),5)
1120 TS2$=LEFT$(STR$(TW2),5)
1130 RS1$=LEFT$(STR$(RW1),5)
1140 RS2$=LEFT$(STR$(RW2),5)
1150 HS$=STR$(HP)
1160 S3$=S2$+SP$+A$(IL)+"."+JD$(IK)
1170 MS$=STR$(MP)
1180 PRINT S3$+PS1$+TS1$+RS1$+PS2$+TS2$+RS2$+SP$+MM$(IK)+SP$
+DD$(IK)+HS$+MS$+SH$+SM$
1190 PRINT#2, S3$+PS1$+TS1$+RS1$+PS2$+TS2$+RS2$+SP$+MM$(IK)
+SP$+DD$(IK)+HS$+MS$+SH$+SM$
1200 LPRINT S3$+PS1$+TS1$+RS1$+PS2$+TS2$+RS2$+SP$+MM$(IK)+SP$
+DD$(IK)+HS$+MS$+SH$+SM$
1210 NEXT IL
1220 CLOSE #1
1230 NEXT IK
1240 CLOSE #2
1250 END
```

REFERENCES

Abell, M., National Geodetic Survey, private communication, 1987.

Ashjaee, J., New results on the accuracy of the C/A code GPS receiver, in *Proc. First International Symposium on Precise Positioning with the Global Positioning System, I*, 207-214, U.S. Department of Commerce, Rockville, MD, Apr. 15 to 19, 1985.

Baker, P. J., Global Positioning System (GPS) policy, in *Proc. of the Fourth International Geodetic Symposium on Satellite Positioning, I*, 51-64, Sponsored by the Defense Mapping Agency and the National Geodetic Survey, at Austin, TX, Apr. 28 to May 2, 1986.

Bertiger, W., and S. M. Lichten, Demonstration of 5 to 20 parts per billion repeatability for a continental baseline estimated with multi-day GPS orbits (abstract), *EOS Trans. AGU, 68*, 1238-1239, 1987.

Beutler, G., D. A. Davidson, R. B. Langley, R. Santerre, P. Vanicek, and D. E. Wells, Some theoretical and practical aspects of geodetic positioning using carrier phase difference observations of GPS satellites, *Tech. Rep. 109*, 79 pp., Department of Surveying Engineering, University of New Brunswick, Fredericton, Canada, Jul. 1984.

Beutler, G., W. Gurtner, M. Rothacher, T. Schildknect, and I. Bauersima, Using the Global Positioning System (GPS) for high precision geodetic surveys: highlights and problem areas, in *IEEE PLANS 86 Record*, 243-250, Sponsored by IEEE AES Society, at Las Vegas, Nov. 4-7, 1986.

Bock, Y., R. I. Abbott, C. C. Counselman, S. A. Gourevitch, R. W. King, and A. R. Paradis, Geodetic accuracy of the Macrometer Model V-1000, *Bulletin Géodésique, 58*, 211-221, 1984.

Cannon, E., G. Lachapelle, and C. Goad, Recovery of a 1700-km baseline using dual frequency GPS carrier phase measurements, in *Proc. First International Symposium on Precise Positioning with the Global Positioning System, II*, 593-602, U.S. Department of Commerce, Rockville, MD, Apr. 15 to 19, 1985.

Carter, W. E., D. S. Robertson, and J. R. MacKay, Geodetic radio interferometric surveying: applications and results., *Journal of Geophysical Research, 90*, 4577-4587, 1985.

Davis, R. E., F. S. Foote, J. M. Anderson, and E. M. Mikhail, *Surveying: Theory and Practice*, Sixth Edition, 992 pp., McGraw-Hill, New York, 1986.

Defense Mapping Agency, Department of Defense World Geodetic System 1984, *DMA Tech. Rep. 8350.2*, 121 pp., Washington, DC, 1987.

Federal Geodetic Committee, *Standards and Specifications for Geodetic Control Networks*, 34 pp., National Geodetic Information Center, NOAA, Rockville, MD, 1984.

Federal Geodetic Committee, *Proposed Geometric Geodetic Survey Standards and Specifications for Geodetic Surveys Using GPS Relative Positioning Techniques*, 50 pp., National Geodetic Information Center, NOAA, Rockville, MD, 1986.

Fell, P. J., The use of standard weather values and refraction bias parameters in orbit determination, *The Canadian Surveyor, 29(3)*, 301-305, Sep. 1975.

Fell, P. J., Geodetic Positioning using a Global Positioning System of satellites, *Reports of the Department of Geodetic Science, Report No. 299*, 279 pp., The Ohio State Research Foundation, Columbus, OH, Jun. 1980.

Goad, C. C., and L. Goodman, A modified Hopfield tropospheric refraction correction model (abstract), *EOS Trans. AGU, 55*, 1106, 1974.

Goad, C. C., and B. W. Remondi, Initial relative positioning results using the Global Positioning System, *Bulletin Géodésique, 58*, 193-210, 1984.

Goad, C. C., M. L. Sims, and L. E. Young, A comparison of four precise Global Positioning System geodetic receivers, *IEEE Trans. on Geoscience and Remote Sensing, GE-23(4)*, 458-465, 1985.

Henson, D. J., and E. A. Collier, Effects of the ionosphere on GPS relative geodesy, in *IEEE PLANS 86 Record*, 230-237. Sponsored by IEEE AES Society, at Las Vegas, Nov. 4-7, 1986.

Hothem, L. D. and G. E. Williams, Factors to be considered in development of specifications for geodetic surveys using relative positioning GPS techniques, in *Proc. First International Symposium on Precise Positioning with the Global Positioning System, II*, 633-644. U.S. Department of Commerce, Rockville, MD, Apr. 15 to 19, 1985.

Jorgensen, P. S., Navstar/Global Positioning System 18-satellite constellation, in *Global Positioning System, II*, 1-12. Institute of Navigation, Washington, DC, 1984.

King, R. W., E. G. Masters, C. Rizos, A. Stolz, and J. Collins, *Surveying with GPS*, 128 pp., School of Surveying, The University of New South Wales, Kensington, N.S.W, Australia, 1985.

Kumar, M., Defense Mapping Agency Hydrographic Topographic Center, letter to the author, dated Feb. 10, 1988.

Landau, H., and B. Eissfeller, Optimization of GPS satellite selection for high precision differential positioning, in *GPS Research at the Institute ... Astronomical and Physical Geodesy*, edited by H. Landau, B. Eissfeller, and G. W. Hein, 65-105, University FAF, Munich, FRG, 1985.

Langley, R. B., G. Beutler, D. Delikaraoglou, B. Nickerson, R. Santerre, P. Vanicek, and D. E. Wells, Studies in the application of the Global Positioning System to differential positioning, *Department of Surveying Engineering Tech. Rep. 108*, 266 pp., University of New Brunswick, Fredericton, Canada, 1985.

Lichten, S. M., and J. S. Border, Strategies for high-precision Global Positioning System orbit determination, *Journal of Geophysical Research, 93(B12)*, 12751-12762, Nov. 10, 1987.

Mader, G. L., and M. D. Abell, A comparison between Global Positioning System and Very Long Baseline Interferometry Surveys in Alaska and Canada, in *Proc. First International Symposium on Precise Positioning with the Global Positioning System, II*, 549-556. U.S. Department of Commerce, Rockville, MD, Apr. 15 to 19, 1985.

Martin, E. H., User equipment error models, *Global Positioning System, I*, 109-118, Institute of Navigation, Washington, DC, 1980.

Milliken, R. J., and C. J. Zoller, Principle of operation of NAVSTAR and system characteristics, in *Global Positioning System, I*, 3-14. Institute of Navigation, Washington, DC, 1980.

Rathacher, M., G. Beutler, and W. Gurtner, The 1985 Swiss GPS -Campaign,in *Proc. of the Fourth International Geodetic Symposium on Satellite Positioning, 2*, 979-991. Sponsored by the Defense Mapping Agency and the National Geodetic Survey, at Austin, TX, Apr. 28 to May 2, 1986.

Remondi, B. W., Using the Global Positioning System (GPS) phase observable for relative geodesy: modelling, processing, and results, Ph.D. Dissertation, 361 pp., The University of Texas at Austin, May 1984.

Remondi, B. W., Global Positioning System carrier phase: description and use, *Bulletin Géodésique, 59*, 361-377, 1985.

Russell, S. S., and J. H. Schaibly, Control segment and user performance, in *Global Positioning System, I*, 74-102. Institute of Navigation, Washington, DC, 1980.

Smith, C. A., Ionospheric total electron content estimation for single-frequency Global Positioning System receivers, Ph.D. Dissertation, 111 pp., University of California, Los Angeles, 1987.

Space Environment Services Center, *Preliminary Report and Forecast of Solar Geophysical Data*, SESC PRF's 631 through 640, Boulder, CO, 06 Oct. to 08 Dec. 1987.

Spilker, J. J., GPS signal structure and performance characteristics, in *Global Positioning System, I*, 29-54. Institute of Navigation, Washington, DC, 1980.

Trimble Navigation, *Trimble Model 4000SX GPS Surveyor - PRELIMINARY - Installation and Operation Manual Rev. 8 1 87*, 96 pp., Sunnyvale, CA, 1987a.

Trimble Navigation, *TRIMVEC GPS Survey Software Preliminary User's Manual, Rev. B*, 62 pp., Sunnyvale, CA, 1987b.

Wells, D. E. (Ed.), *Guide to GPS Positioning*, Canadian GPS Associates, Fredericton, New Brunswick, Canada, 1986.

INITIAL DISTRIBUTION LIST

		No. Copies
1.	Defense Technical Information Center Cameron Station Alexandria, VA 22304-6145	2
2.	Library, Code 0142 Naval Postgraduate School Monterey, CA 93943-5002	2
3.	Chairman (Code 68Co) Department of Oceanography Naval Postgraduate School Monterey, CA 93943	1
4.	Prof. Stevens P. Tucker Department of Oceanography (Code 68Tx) Naval Postgraduate School Monterey, CA 93943	3
5.	Prof. Narendra K. Saxena Department of Civil Engineering University of Hawaii at Manoa 2540 Dole Street, Holmes 383 Honolulu, HI 96822	3
6.	LT Richard H. Bouchard, USN NAVOCEANCOMCEN JTWC COMNAVMARIANAS Box 12 FPO San Francisco 96630-2926	3
7.	Director Naval Oceanography Division Naval Observatory 34th and Massachusetts Avenue NW Washington, DC 20390	1
8.	Commander Naval Oceanography Command NSTL Station Bay St. Louis, MS 39522	1
9.	Commanding Officer Naval Oceanographic Office NSTL Station Bay St. Louis, MS 39522	1

10. Commanding Officer — 1
Naval Ocean Research and Development Activity
NSTL Station
Bay St. Louis, MS 39522

11. Chairman, Oceanography Department — 1
U.S. Naval Academy
Annapolis, MD 21402

12. Chief of Naval Research (Code 420) — 1
Naval Ocean Research and Development Activity
800 N. Quincy Street
Arlington, VA 22127

13. Director (Code PPH) — 1
Defense Mapping Agency
Bldg. 56, U.S. Naval Observatory
Washington, DC 20305

14. Director (Code HO) — 1
Defense Mapping Agency Hydrographic Topographic Center
6500 Brookes Lane
Washington, DC 20315

15. Director (Code PSD-MC) — 1
Defense Mapping School
Ft. Belvoir, VA 22060

16. Director, Charting and Geodetic Services (N CG) — 1
National Ocean and Atmospheric Administration
Rockville, MD 20852

17. Chief, Program Planning, Liaison and Training (NC2) — 1
National Oceanic and Atmospheric Administration
Rockville, MD 20852

18. LTJG James Waddell, NOAA — 1
SMC 2590
Naval Postgraduate School
Monterey, CA 93943

19. Mr. Gary Fredrick — 1
NOAA, NOS
Code N/MOP 222
Bin C15700
7600 Sand Point Way, NE
Seattle, WA 98115-0070

20. Mr. Paul Perrault — 1
Trimble Navigation, Ltd.
585 North Mary Avenue
Sunnyvale, CA 94088-3642

21. Ma, Wei-Ming 1
SMC 2229
Naval Postgraduate School
Monterey, CA 93943

22. Dr. Stephen M. Lichten 1
Jet Propulsion Laboratory
California Institute of Technology
Mail Stop 238-640
4800 Oak Grove Drive
Pasadena, CA 91109

END

DATE

FILMED

8-88

DTIC